

Imperial College London

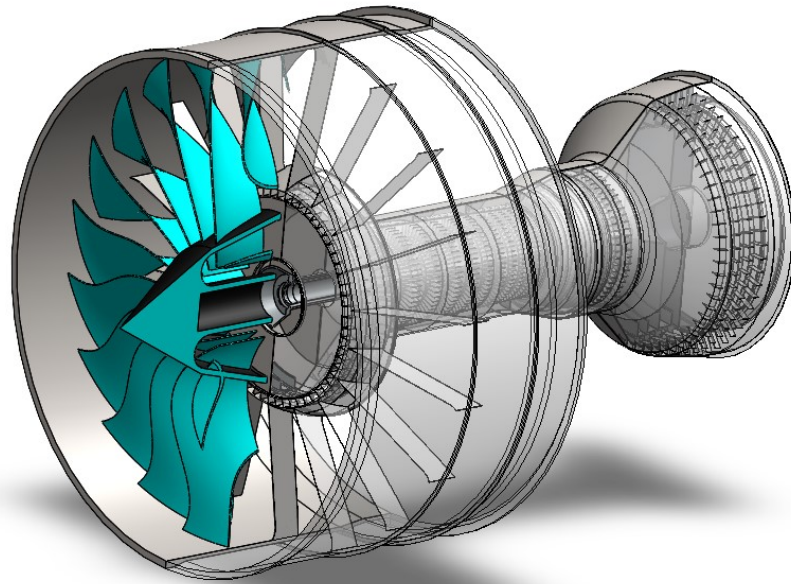
Department of Mechanical Engineering

**Aircraft Engine Technology: Task 3**

---

**Engine Sizing of a Fire-Tanker Aircraft**

---



*Group 2:*

Areeb Nasim Haider *AHaider*  
Conor Leo *ConorLeo*  
Diederik Evanson *DEvanson*  
Rohit Nag *RohitNag*

*Supervisor:*

Prof. Ricardo Martinez-Botas

We declare that equal contribution has been made by all group members for this project, and we agree to an equal distribution of marks.

March 20, 2023

## Abstract

Fire fighting aircraft are often used to extinguish bush fires in Australia due to the vast area covered by fire and the lack of local water sources. *The Air Tanker* is a new aircraft designed to transport 30 tonnes of water from a local airport, drop it on a fire up to 1500 km away and return to the airport to refill.

*The Air Tanker* utilises two, medium-bypass, two-spool, unmixed Turbofan engines which were optimised for a low Specific Fuel Consumption (*SFC*) and a high Specific Thrust ( $\frac{T}{m}$ ) at cruise. The two engines each have a diameter of 2.6m with a bypass ratio of 7 and produce a thrust of 53.2 kN at cruise from a mass flow rate through the core of just 20.5 kg/s. Despite the focus being on optimising for low *SFC* and high Specific Thrust, the engine designed was also efficient at cruise conditions, reaching core and propulsive efficiencies of 57.6% and 73.3% respectively.

Several off-design conditions were considered: take-off of the aircraft with both engines functioning; take-off with only one engine functioning; and the aircraft at top of climb. The engines can deliver a maximum thrust of 237.0 kN under take-off conditions without surpassing material temperature limits. This is enough to fulfil the thrust requirements for all of the off-design conditions.

The engine was primarily composed of a fan and a low pressure booster, a high pressure compressor, a high pressure turbine and a low pressure turbine. The low pressure compression stage has two booster stages and spins at an angular velocity of 294.67  $rads^{-1}$  and has an overall pressure ratio of 2.5. The high pressure compression stage has 11 stages, each with a pressure ratio of 1.29 and spins at 850  $rads^{-1}$  giving an overall compression ratio of 16. These were powered by the high pressure turbine which had 3 stages and an overall pressure ratio of 5.63, in conjunction with the low pressure turbine which had 4 stages, with an overall pressure ratio of 6.73. These parameters produced a design with a total-to-total efficiency of 89% for the high pressure turbine and 87% for the low pressure turbine at cruise.

The blade angles for the compressors and turbines were designed to maximize efficiency. The stresses in the HP disks were analyzed and determined to have a minimum safety factor of 1.52. Finally, the thickness of the disk was optimised so that unnecessary mass was removed.

This report details the process followed to design the engines for *The Air Tanker*.

## Contents

<b>1 Engine Drawing</b>	<b>1</b>
<b>2 Introduction</b>	<b>2</b>
<b>3 Initial Design Choices</b>	<b>2</b>
<b>4 Operating Conditions</b>	<b>3</b>
<b>5 On-Design Optimisation</b>	<b>7</b>
<b>6 Off-Design Verification</b>	<b>12</b>
<b>7 Fan Design</b>	<b>13</b>
<b>8 Compressor Design</b>	<b>14</b>
<b>9 Turbine Design</b>	<b>17</b>
<b>10 Compressor Blade Design</b>	<b>20</b>
<b>11 Turbine Blade Design</b>	<b>23</b>
<b>12 Parameter Optimisation Algorithm</b>	<b>27</b>
<b>13 Stress Analysis</b>	<b>28</b>
<b>14 Further Development</b>	<b>31</b>
<b>15 Conclusion</b>	<b>32</b>
<b>References</b>	<b>33</b>
<b>A Appendix</b>	<b>35</b>

# 1 Engine Drawing

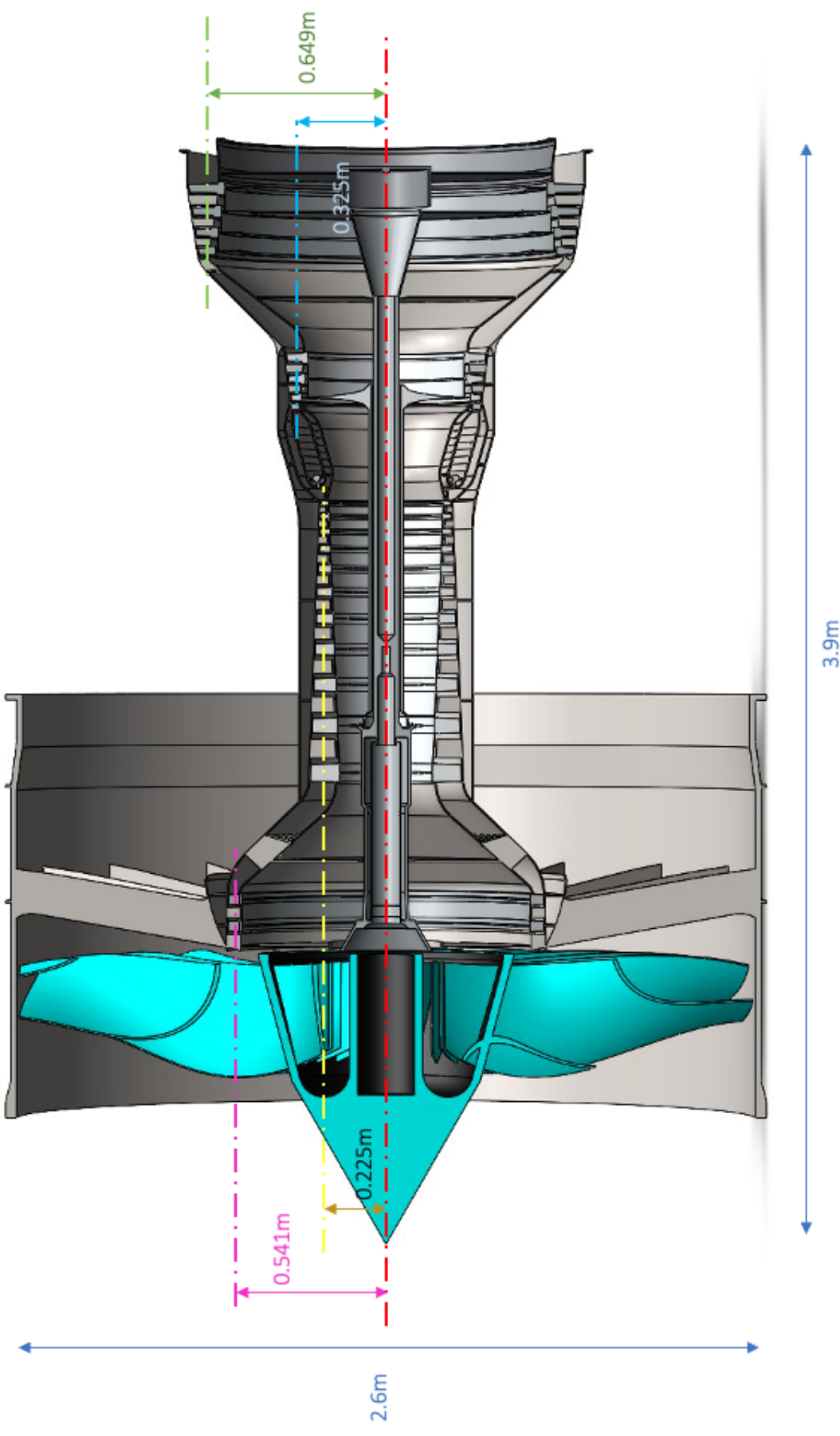


Figure 1: To Scale Engine Cross Section.

## 2 Introduction

Forest fires are common in Australia due to the hot, dry climate, and firefighting aircraft are often used to extinguish these fires. The aircraft drops liquid fire retardants onto the affected areas from the air. Traditional fire trucks are often ineffective as they are limited by their speed and capacity. By contrast, aircraft can be quickly deployed from the closest town with an airfield, and carry large volumes of fire retardant. The objective of this report is to design the engines used in a firefighting aircraft deployed in Australia named *The Air Tanker*.

### 2.1 Duty Requirements

There are various types of firefighting aircraft suited for different applications. Single Engine Airtankers (SEATs) such as the *Air Tractor AT-802* are designed to operate in areas that are difficult for larger aircraft to access. These aircraft are limited to 800 gallons of fire retardant [1]. Large Airtankers (LATs) are the most common, delivering 3000 gallons of fire retardant [1]. Very Large Airtankers (VLATs) such as the specialized *Boeing 474* can carry up to 24000 gallons of fire retardant [2]. VLATs are rarely deployed due to significant operational costs and long deployment times. Some of these aircraft also need to reload and refuel at aerial firefighting bases, limiting their effectiveness.

Considering the immense area of fire, the aircraft must carry a large volume of liquid. Despite this, accounting for the short fully-laden flight distances and the requirement to refill at small airports, the aircraft cannot have the specialised reloading equipment and long deployment times characteristic of VLATs. Therefore, *The Air Tanker* will be designed to transport a payload of 30 metric tonnes, sized between traditional LATs and VLATs. Since water is more readily available at remote locations compared with sources of liquid fire retardant, *The Air Tanker* will be designed to carry water as the fire-fighting fluid.

The maximum range required of *The Air Tanker* is from the coast of Australia to the center (5000 km). Considering the high likelihood of a small airport existing closer to the fire, the *The Air Tanker* will be designed to fly 3000 km. Only on the outbound journey will the aircraft be fully-laden as the aircraft will drop the payload at the fire.

The three primary phases of the flight that the engine must handle are: take-off and climb, loaded and unloaded cruise, and landing. Outbound cruise will be considered the on-design condition as the aircraft's main purpose is to transport water to the fire.

Issues common to many aircraft are not of concern for *The Air Tanker* such as take-off noise since take-off will be distant from populated regions, as well as reducing the price per flight given the aircraft will be deployed infrequently and the monetary benefits for extinguishing bush fires far out weigh the incremental benefits of decreasing the price per flight. *The Air Tanker* needs to be fuel efficient to maximise water capacity. Thus the optimising parameters for the *The Air Tanker* will be twofold: minimising the Specific Fuel Consumption (*SFC*) and maximizing the Specific Thrust ( $\dot{T}$ ).

## 3 Initial Design Choices

First, deciding on the engine type (turboprop, turbofan or turbojet) is critical. The cruise Mach number 0.84 is too high for a conventional turboprop engine. Additionally, the Specific Fuel

Consumption (*SFC*) of advanced turboprop engines at this velocity are considerable and some designs may not operate at all. Turbojet engines can handle this velocity and have high thrust to airflow ratios. However, they are also characterised by a high *SFC* which would require *The Air Tanker* to sacrifice water for fuel. Turbofans operate well at the required velocity and have a far lower *SFC* than turbojet engines balanced against a lower thrust to airflow ratio than turbojets. Thus, *The Air Tanker* will use a turbofan design given its suitability to our proposed application. Actual values of *SFC* and specific thrust vary considerably depending on the bypass ratio of the engine.

Second, modern engines can feature two or three coaxial shafts. A three-spool design is more efficient at the cost of greater complexity and weight. *The Air Tanker* will have a two-spool design as the slight efficiency benefits do not outweigh the advantages of reduced complexity and weight savings. *The Air Tanker* will be operating over bush-fires where above-average quantities of ash and smoke are expected to be ingested. This will require more frequent servicing than commercial aircraft, favouring simplicity of design. Additionally, *The Air Tanker* is only used for short periods so the incremental increase in efficiency is not as beneficial as it would be for commercial aircraft.

Third, the number of engines on the aircraft must be chosen, typically two or four. This choice primarily affects the off-design case of a single engine failure. In such situations, the aircraft must take off using the remaining engines. *The Air Tanker* will be a two engine design, primarily to save on down-time and cost due to maintenance.

Finally, the Nacelle of the engine can be mixed or unmixed. *The Air Tanker* will be unmixed to save on weight and nacelle drag. As discussed, a greater noise production is acceptable due to the *The Air Tanker*'s non-commercial use and remote operation.

## 4 Operating Conditions

*The Air Tanker* is designed to take off from an airport at sea level. The minimum climb angle is  $3^\circ$  [3]. *The Air Tanker* will be designed with a take off angle of  $5^\circ$  until it reaches the standard cruise height of 35,000 ft. *The Air Tanker* will descend at an angle of  $5^\circ$  to 400-800 ft for precise water discharge, cruising for less than a minute before climbing again at a  $5^\circ$ . This will be considered an additional take off and landing thus it will not be analysed separately. The expected mission profile is shown in Figure 2.

Minimising the weight of fuel consumed per unit distance requires that  $\frac{ML}{D}$  be maximised [3]. From Figure 3,  $\frac{ML}{D}$  is maximised at approximately Mach 0.84. This subsonic velocity will be the cruise velocity for *The Air Tanker*. Ultimately, the objective is to increase the mass of water transported per unit time. The aircraft could be designed to fly faster but the costs would outweigh the benefits. The decision to reduce flight speed and increase payload is preferred. The wing will be designed to have a  $C_L$  of around 0.5 at cruise. This will give an  $\frac{ML}{D}$  value of approximately 17.5 which is comparable to similar aircraft.

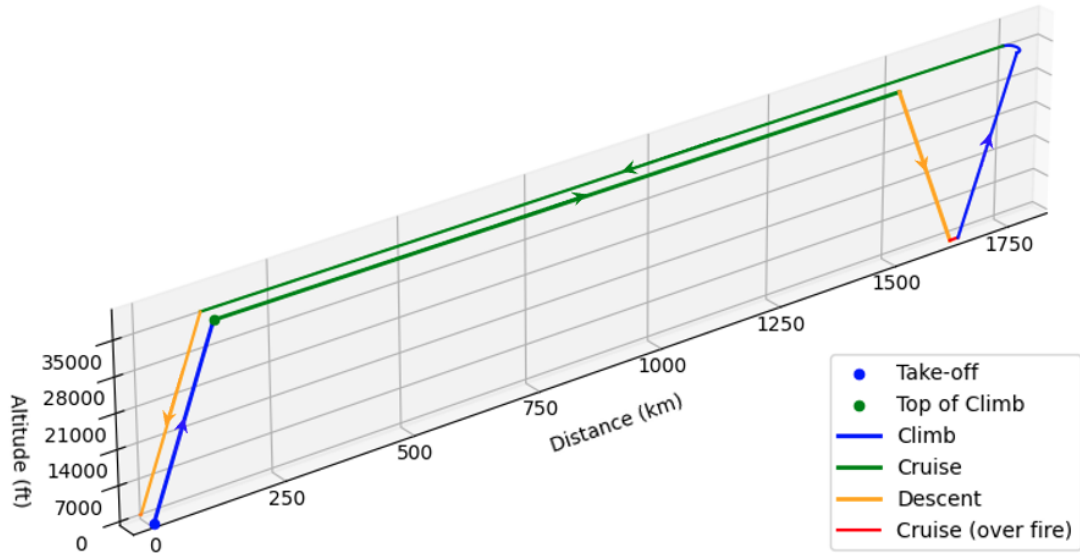


**Figure 2:** Expected mission profile of *The Air Tanker*. Bold lines indicate full payload.

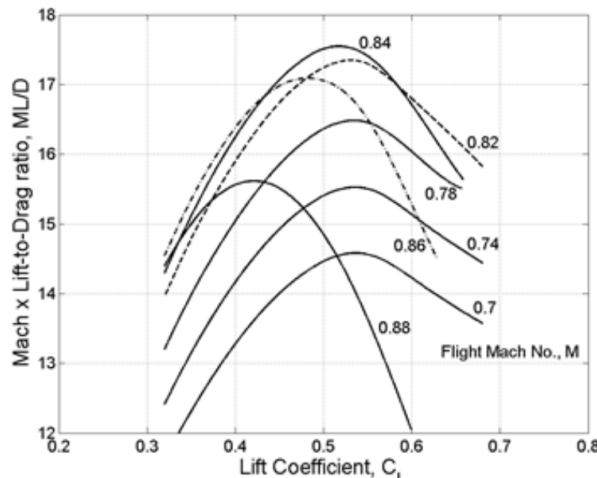


**Figure 3:** Relationship between  $\frac{ML}{D}$  and  $C_L$  with varying Mach numbers for similar aircraft.  
[4]

#### 4.1 Weight of Aircraft

The total weight is one of the primary factors dictating the thrust required from the engine. This is the combined weight of the empty aircraft, the fuel and the transported water. Therefore, an estimate of the fuel requirements and the empty aircraft weight is needed. These estimates will come from analysis of similar aircraft.

As discussed in Section 2.1, *The Air Tanker* is designed to transport 30 tonnes of water for a distance of 1500 km before releasing the payload and traveling another 1500 km with no payload. This duty case is similar to the range and maximum payload of the Airbus A300-B2, the Airbus A300-600 and the Boeing 767-200. Their relevant properties are displayed in Table 1.

*The Air Tanker* is most similar to the Airbus A300-B2 in terms of requirements, however the Airbus A300-B2 was entered into service in 1974 and aircraft technology has progressed significantly since then in terms of empty weight and fuel efficiency. Additionally, *The Air*

**Table 1:** Properties of Relevant Aircraft. (\* indicates a calculated value) [4]

Parameters	Airbus A300-B2	Airbus A300-600	Boeing 767-200	The Air Tanker
Maximum Range [NM]	1500	3100	4000	1619
Empty Weight [t]	86	87	80	80
Max Payload [t]	30.6	43.3	33.2	30
Weight of Fuel [t]	20.4*	34.7*	29.8*	17
Max Take-Off Weight [t]	137	165	143	127*

*Tanker* only transports its payload half of the total distance. Thus it will be designed with an empty weight of 80 tonnes and a fuel requirement of 17 tonnes. These values combine to give a maximum take-off weight of 127 tonnes.

## 4.2 Lift to Drag Ratio

In Section 4, the Mach number of cruise was chosen to be 0.84 which gave a  $\frac{ML}{D}$  value of 17.5. From this equation, the lift-to-drag ratio ( $\frac{L}{D}$ ) is calculated to be 20.8 at cruise conditions, standard for modern aircraft.

The lift-to-drag ratio of *The Air Tanker* at take-off is more difficult to determine as the aircraft has a far lower Mach number. Literature indicates that  $\frac{L}{D}$  at take-off will be approximately 10 [5].

$\frac{L}{D}$  is a function of multiple parameters, however for simplification, the variation at different points in the flight path will be assumed to be encapsulated by the change in normalised altitude ( $\hat{H}$ )<sup>1</sup>. It is assumed that  $\frac{L}{D}$  varies linearly with  $\hat{H}$  and can be defined by Equation 1. This is derived from the respective  $\frac{L}{D}$  values at take-off and cruise.

$$\frac{L}{D} = 10.8\hat{H} + 10 \quad (1)$$

## 4.3 Thrust

The required thrust for steady flight is calculated from a force balance, shown in Figure 4. To generalize calculations for different conditions, the aircraft is assumed to be travelling opposite to the airflow at a velocity ( $v$ ) with a climb angle ( $\gamma$ ) and weight  $W$  (see Section 4.1). The drag ( $D$ ) acts in the direction of the free stream velocity ( $v_\infty$ ) while lift acts perpendicular to  $v_\infty$ . The thrust ( $T$ ) is assumed to act at an angle,  $\alpha_T$ , to the flight path.

The force-balances in the x and y-directions as shown in Equations 2 and 3 can be rearranged in-terms of the  $\frac{L}{D}$ , a known value at key operating points (see Section 4.2).

$$\Sigma F_x = 0 \Rightarrow D = T \sin(\alpha_T) - W \sin(\gamma) \quad (2)$$

$$\Sigma F_y = 0 \Rightarrow L = W \cos(\gamma) - T \sin(\alpha_T) \quad (3)$$

Assuming thrust angle is small ( $\alpha_T \approx 0$ ), Equation 4 gives a general expression for the required thrust found from the force-balances. This can be further modified to find the required

<sup>1</sup> $\hat{H}$  has a value of 1 at top of climb, and 0 at take-off.

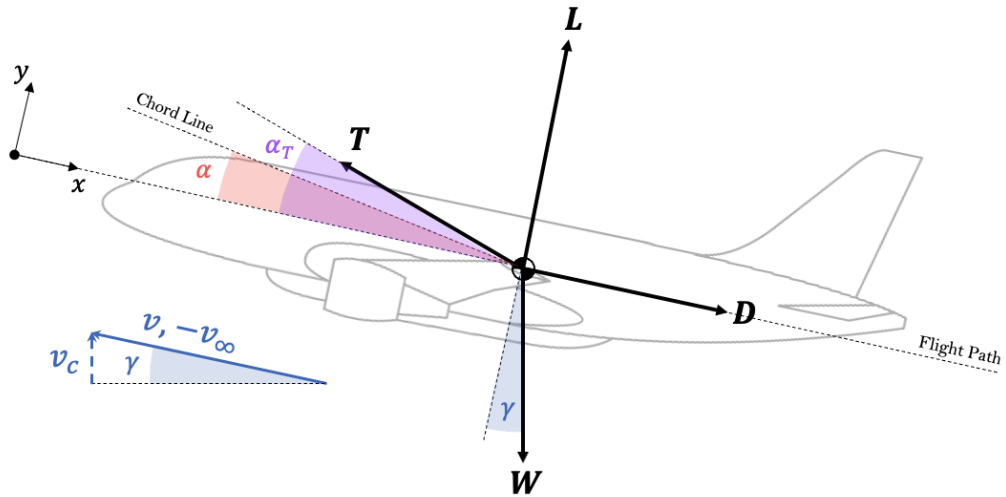


**Figure 4:** Generalised free body diagram of the aircraft

thrust at different operating conditions as discussed in following subsections.

$$T_R = W \left[ \left( \frac{L}{D} \right)^{-1} \cos(\gamma) + \sin(\gamma) \right] \quad (4)$$

#### 4.3.1 Take Off Thrust

The aircraft will be taking-off at approximately 170 mph<sup>2</sup> from sea-level at a climb angle of 5°.  $\frac{L}{D}$  can be approximated to value of 10 as discussed in Section 4.2. The weight of the aircraft will be the greatest at this operating point, equal to  $MTOW \cdot g$  as defined in Table 1. Using Equation 4 and the take-off parameter values, the required thrust at take-off ( $T_{R_{TO}}$ ) is found to be **116 kN per engine**.

For a single engine failure at take-off, the net thrust has to be provided by the remaining engine. In such a scenario, the required thrust will be **232 kN per engine**.

#### 4.3.2 Climb Thrust

During climb, the aircraft will lose weight due to combustion. For a conservative calculation, the weight used will be equal to that at take-off. Using Equation 1, the required thrust equation can be written as a function of  $\hat{H}$  as shown in Equation 5.

$$T_R(\hat{H}) = W \left[ \frac{\cos(\gamma)}{10.8\hat{H} + 10} + \sin(\gamma) \right] \quad (5)$$

The climb phase is defined as the phase between take-off ( $\hat{H} = 0$ ) and top of the climb ( $\hat{H} = 1$ ). Thus, the above expression can be integrated over the interval  $\{0, 1\}$  to find the average climb thrust ( $\bar{T}_C$ ) using Equation 6.

$$\begin{aligned} \bar{T}_C &= \int_0^1 T_R(\hat{H}) d\hat{H} \\ &= W \left[ \sin(\gamma) + \frac{5}{54} \cos(\gamma) \ln \left( \frac{52}{25} \right) \right] \end{aligned} \quad (6)$$

The average thrust to maintain a steady climb at 5° is **96.4 kN per engine**.

---

<sup>2</sup>Takeoff speed generally lies in the range of 160-180 mph [6]. 170 mph was chosen given it matches the takeoff speed of comparably-sized aircraft. This corresponds to mach number of 0.22 at sea level.

### 4.3.3 Top of Climb Thrust

Top of climb has been defined as the point where the aircraft reaches cruise altitude and is climbing with a climb angle of  $5^\circ$ .  $\frac{L}{D}$  is 20.8 at this point, resulting in a **required thrust of 84 kN per engine** from Equation 4.

### 4.3.4 Cruise Thrust

At cruise, the climb angle ( $\gamma$ ) is zero and  $\frac{L}{D}$  is 20.8. Thus, the **thrust per engine is 29.9 kN per engine** from Equation 4.

## 4.4 Summary of Operating Parameters

Table 2 summarises the on-design and off-design operating parameters.

**Table 2:** Summary of Operating Parameters

Parameters	Take-off		Top of Climb	Laiden Cruise
	Normal	<i>Engine Failure</i>		
Height [ft]	0	0	35,000	35,000
$\hat{H}$	0	0	1	1
$P_a$ [kPa]	101.3	101.3	23.8	23.8
$T_a$ [K]	288.15	288.15	218.8	218.8
$\gamma$ [ $^\circ$ ]	5	5	5	0
Mach Number	0.22	0.22	0.84	0.84
$L/D$	10	10	20.8	20.8
$T_R$ per Engine [kN]	<b>116</b>	<b>232</b>	<b>84</b>	<b>29.9</b>

## 5 On-Design Optimisation

### 5.1 Practical Constraints

The material thermal limit for turbines is 1850 K [7] for short time periods. This sets the Turbine Entry Temperature (*TET*) limit. Likewise, the Compressor Delivery Temperature should not exceed 950 K [7]. The overall pressure ratio is limited by the size and temperature of the compressor blades. The blades should not be smaller than 10 mm. For large engines, this limits the overall pressure ratio to 40 [7].

The engine must fit between the wing and the ground with a 0.5 m clearance. As discussed in Section 5.1, the aircraft is most similar to the *Airbus A300-B2* aircraft which has a ground clearance of 4.19 m measured from the underside of the wing [8]. The current largest commercial turbofan, the *Rolls-Royce Ultrafan* has an engine diameter 3.556 m [9]. A diameter larger than this would require raising wing position or raising the fuselage, causing interfacing issues with airport machinery. Hence 3.556 m will be used as the maximum engine diameter.

The engine also requires cooling air to be siphoned off after the high pressure compressor and gets re-added to the gas stream before the high pressure turbine as shown in the engine diagram in Appendix A.1. There is also a 5% Nozzle Guide Vane (NGV) cooling and a 6% HP Turbine cooling from the compressed air at 1468kPa.

## 5.2 Efficiency Assumptions

Table 3 shows the isentropic efficiencies [10] used for calculations in GasTurb 10.

**Table 3:** Efficiencies used in GasTurb 10

	Intake	Fan	LPC	HPC	LPT	HPT
Efficiency	0.97	0.91	0.91	0.91	0.92	0.92

## 5.3 Turbine Entry Temperature

The Turbine Entry Temperature (*TET*) must be significantly below 1850 K at cruise as discussed in Section 5.1. The exact temperature was chosen via Figure 5.

It is important to note the distinction between the burner exit temperature T4 and the Turbine Entry Temperature (TET), as GasTurb uses the burner exit temperature as its input (see Figure 17). Due to 6% HP Turbine cooling (GasTurb default) there is a temperature drop between the combustor exit and the turbine entry.

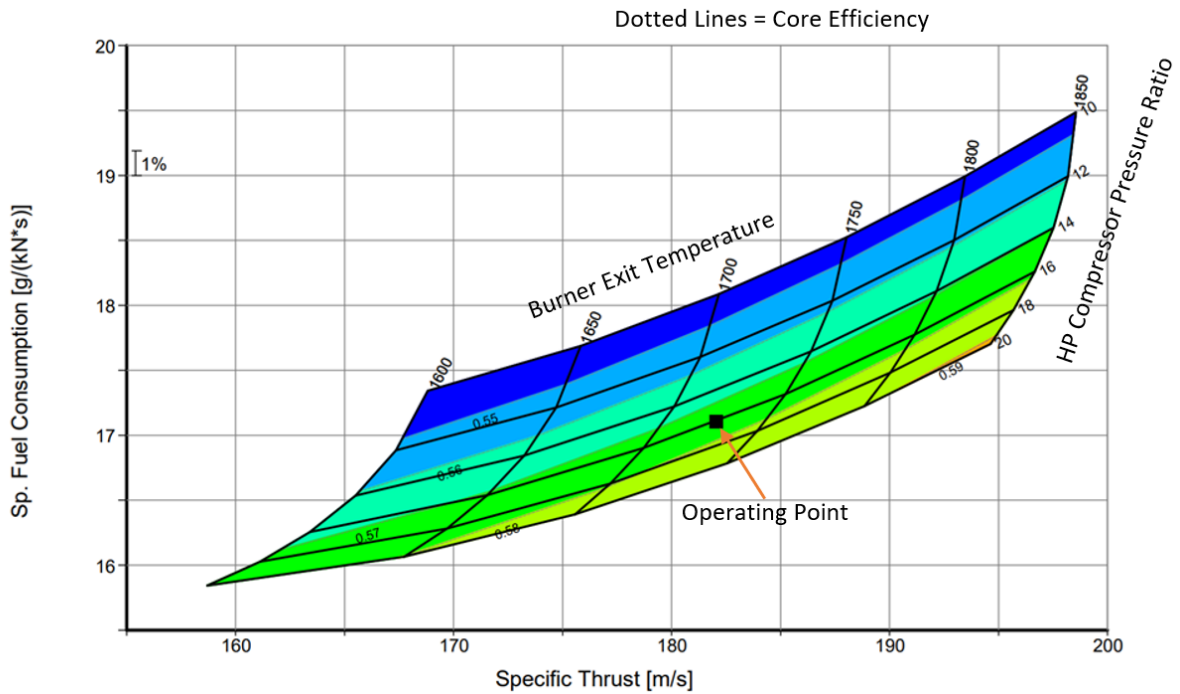


**Figure 5:** The relationship between specific fuel consumption of the engine and the specific thrust with varying turbine entry temperatures, HP compressor pressure ratios and efficiency.

The chosen operating point is indicated.

For large High Pressure Compressor ratios, the minimum SFC is found at a burner exit temperature 1600 K. The iteration process detailed in Section 5.8 produced a burner exit temperature of 1725 K which significantly increases the specific thrust and core thermal efficiencies. The *SFC* however, only increases slightly. This trade off was deemed to be worthwhile, thus the burner exit temperature at cruise was chosen to be 1725 K. There is cooling between burner and the turbine entrance, so the **TET will be 1678 K**. This is acceptable provided the temperature does not exceed 1850 K during any off-design conditions. Off-design conditions are verified in

Section 6.

#### 5.4 Overall Pressure Ratio

The overall pressure ratio (*OPR*) is limited to approximately 40 as explained in Section 5.1. Figure 6 shows how the chosen optimisation parameters (*SFC* and  $\dot{T}$ ) and the core thermal efficiency vary with *OPR*.

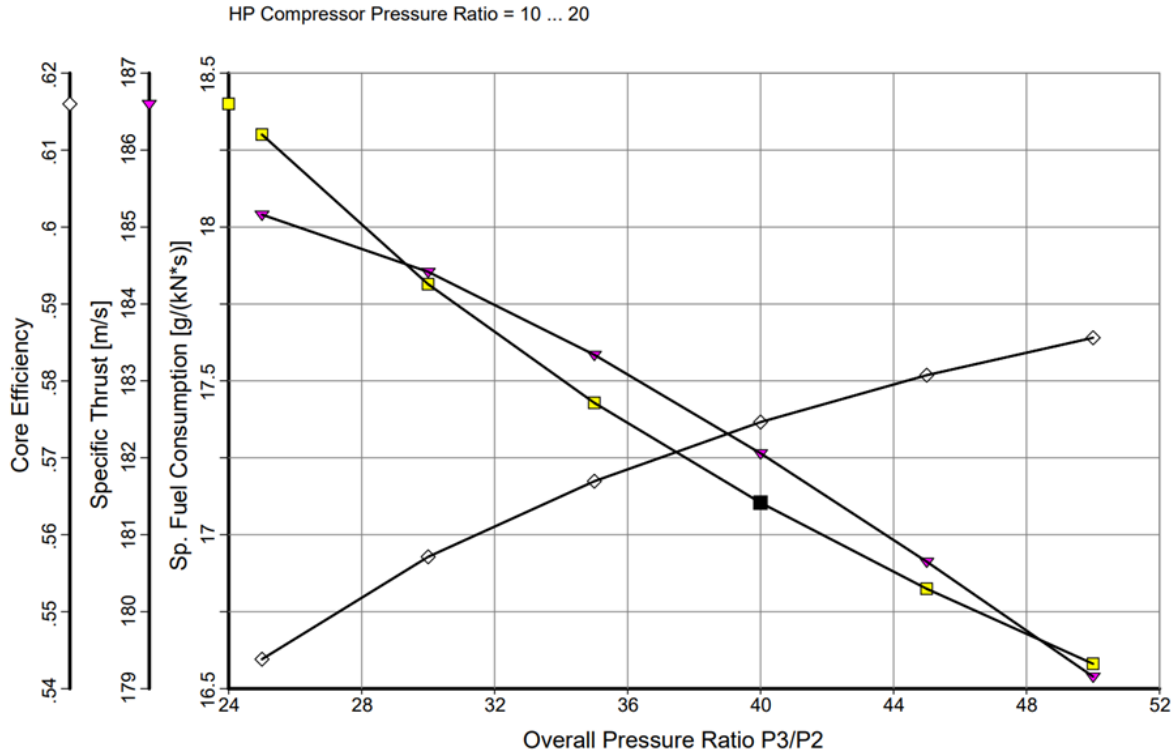


**Figure 6:** Graph of Critical values against *OPR*

Specific fuel consumption and core thermal efficiency increases at higher *OPR* while specific thrust decreases. It should also be noted that larger *OPR* increases the weight of the engine, decreasing performance. Specific fuel consumption was valued more than the specific thrust, thus the *OPR* was chosen to be as high as practical at 40.

#### 5.5 Low Pressure Compressor Pressure Ratio

The Low Pressure Compressor (LPC) pressure ratio was taken from literature, giving values between 1 and 2.5 for 2-spool engines without a gearbox between the fan and low pressure shaft [4]. It is beneficial to have small pressure ratios for the High Pressure Compressor to reduce the number of compressor stages. Fewer stages result in lower weight, increasing the engine's efficiency. A simpler compressor also reduces the time spent in maintenance. A small *HPC* pressure ratio relies on a large *LPC* pressure ratio, thus the *LPC* pressure ratio was set to 2.5.

#### 5.6 Outer Fan Pressure Ratio

The specific fuel consumption and specific thrust vary with outer fan pressure ratio (*OFPR*). Figure 7 shows this variation along with its dependency on the *BPR*.

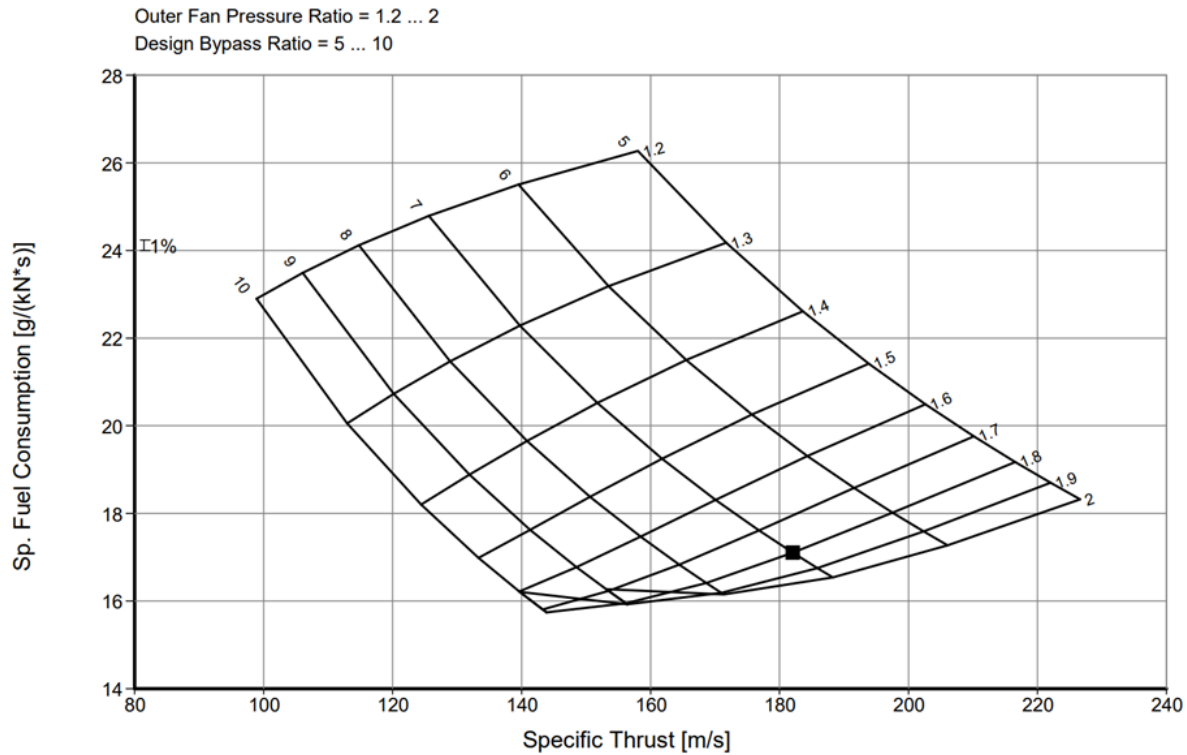


**Figure 7:** Relationship between  $SFC$  and  $\dot{T}$  with varying  $BPR$  and  $OFPR$

For the given parameters, Specific Fuel Consumption is never less than 15.8 g/kNs. An  $OFPR$  of 1.8 provides the minimum  $SFC$  while also having high  $\dot{T}$  values. An  $OFPR$  of 2 was considered but rejected because it resulted in a lower propulsive efficiency with only a slight gain in specific fuel consumption.

## 5.7 Bypass Ratio

Figure 7 illustrates that for an  $OFPR$  of 1.8, the bypass ratio significantly affects the specific thrust output while only slightly changing the specific fuel consumption. For this reason, the **BPR was set to 7**. This provides an increase in specific thrust of 40 m/s compared to a  $BPR$  of 10, while only increasing specific fuel consumption by 0.5 g/kNs.

## 5.8 Mass Flowrate and Engine Diameter

The calculation of the engine diameter,  $\phi$  was done via an iterative process, as shown in the flowchart in Figure 8. The design process was intended to find the mass flowrate requirements and size the engine at cruise. The engine diameter would then be used to validate takeoff with an engine failure, the most extreme off-design condition.

To find the mass flowrate at cruise, a value of specific thrust was chosen from Figure 5. The mass flowrate required at cruise was then calculated using Equation 7.

$$\dot{m} = \frac{T_R}{\dot{T}_R} \quad (7)$$

Since GasTurb takes in mass flowrate relative to sea level, it was important to correct the mass flowrate using Equation 8. This input is referred to as **W2Rstd** in GasTurb [11].

$$\dot{m}_{corr} = \dot{m} \frac{P_{sea}}{P_{02}} \sqrt{\frac{T_{02}}{T_{sea}}} \quad (8)$$

Once the mass flowrate at cruise has been calculated, the diameter of the engine can be calculated, noting that at cruise conditions, the air streamlines diverge and decelerate to approximately 0.6 of the free stream velocity [4]. By treating air as a compressible gas, the new local properties were calculated using the compressible flow equations. Finally, the mass flowrate at takeoff conditions can be calculated using Equation 9.

$$\dot{m} = \rho V_\infty A \quad (9)$$

The free stream velocity at takeoff ( $V_\infty$ ) is set between 70-90 m/s [12] depending on the conditions. The density of atmospheric air at takeoff was taken to be  $1.225 \text{ kg m}^{-3}$ .

Again, it is important to note that at takeoff conditions, the streamlines converge when passing through the engine casing, and hence accelerate to approximately 1.67 of the free stream velocity [4].

As most of the engine parameters were fixed, the only variables used to iterate through the process was the engine diameter and the TET.

*The Air Tanker diameter was set to 2.6 m to ensure minimum thrust requirements for all conditions were met. Table 5 shows the final values of the mass flowrates and temperatures for all conditions.*

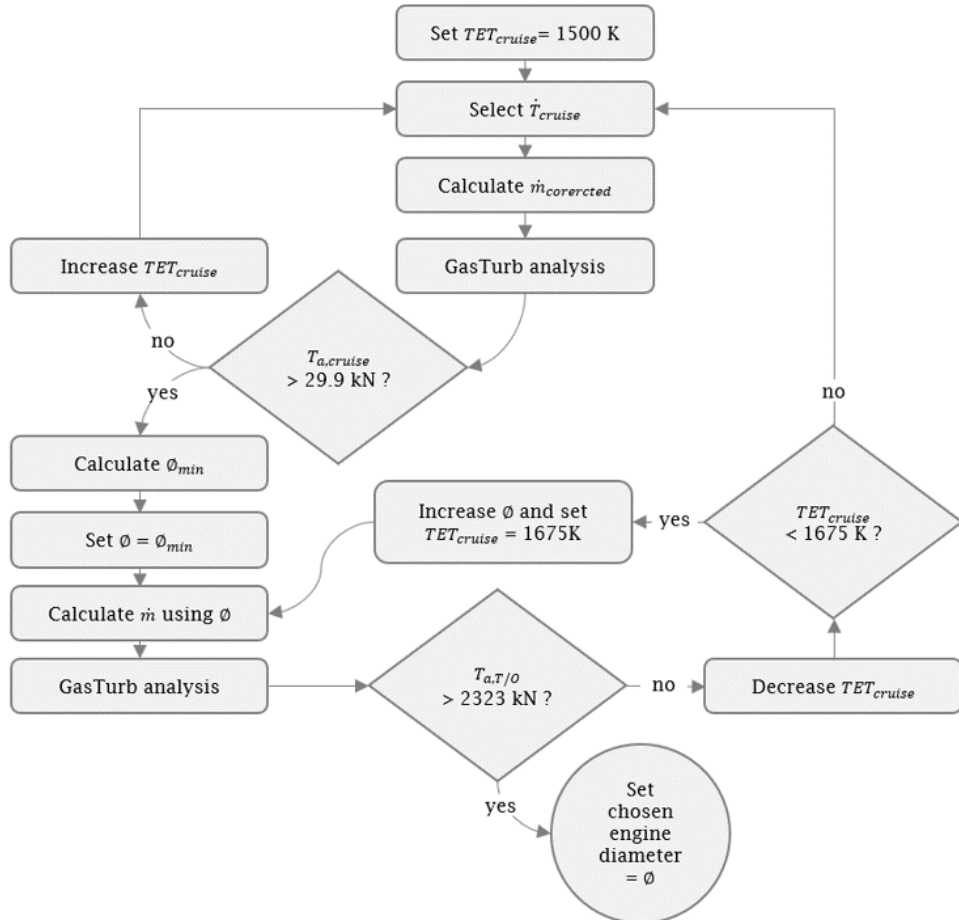


**Figure 8:** Flow chart detailing iterative design methodology

## 6 Off-Design Verification

The engine parameters have been optimised for cruise conditions, however the engine must also be able to perform at off-design conditions. These conditions are: take-off under standard conditions, take-off with single engine failure and top of climb.

The primary factors that must be verified is that the engine can produce the required thrust and the turbine entry temperature is below the thermal material limits. Secondary to that is ensuring the engine diameter allows sufficient ground clearance. It was determined in Section 5.1 that the spacing between the underside of the wing and the ground was 4.19 m. The 2.6 m engine diameter leaves 1.59 m ground clearance which is more than enough to be deemed acceptable.

### 6.1 Take-Off

At take-off, the required thrust per engine is 116 kN, which the engine produces (as it produces 180.9 kN) at a burner exit temperature of 1750 K and a corrected mass flow rate of  $759 \text{ kgs}^{-1}$ . This fits the design requirements as the TET after cooling results in 1706 K, which does not exceed the maximum temperature limitations of the turbine blades.

### 6.2 Top of Climb

Similar to take-off, the required thrust per engine for top of climb is 84 kN, which at a burner exit temperature of 1825 K and a corrected mass flow rate of  $1141 \text{ kgs}^{-1}$ , the engine produces 86.2 kN, just enough to meet the minimum requirements.

### 6.3 Engine Failure

To account for engine failure, the focus was shifted to take-off conditions, as that is the phase of the mission which requires the most thrust<sup>3</sup>. In the event of an engine failure, the remaining engine will be required to produce 232 kN. At a burner exit temperature of 1900 K, the turbine inlet temperature will be 1850 K and a corrected mass flow rate of  $867 \text{ kgs}^{-1}$ , the engine produces a total thrust of 237.0 kN, which is more than sufficient to take off. All of the engine performance metrics are defined in Table 5.

### 6.4 Summary of Engine Parameters

The final design for the aircraft utilises two medium-bypass, two-spool, unmixed turbofan engines. The final parameters for an engine powering *The Air Tanker* are shown in Table 4. An engine with these parameters will perform with the values in Table 5.

---

<sup>3</sup>It is assumed that if the engine is capable of producing the required thrust in this condition, it will be able to cope with engine failure during all stages of its mission.

**Table 4:** Final Engine Parameters

Parameters	Value
Diameter [m]	2.6
Bypass Ratio	7
Overall Pressure Ratio	40
Inner Fan Pressure Ratio	2.5
High Pressure Compressor Ratio	16
Outer Fan Pressure Ratio	1.8

These performance metrics meet the thrust requirements for the duty case. They also ensure that the maximum material temperature is not exceeded and require corrected air mass flow rates that can realistically be provided by an engine with the specified diameter. Thus the engine will be able perform the duty case without failing. Additionally, the engine parameters have been selected to optimise the performance of the engine at cruise. The specific fuel consumption was minimised as far as practical without severely compromising the specific thrust. These choices produce an engine capable of efficiency powering the new fire-fighting aircraft.

**Table 5:** Engine Performance Metrics

Parameters	Take-off	Top of Climb	Laiden	
	Normal		Cruise	
$\dot{T}$ [ $ms^{-1}$ ]	236	270	182	182
Take-Off Speed [ $ms^{-1}$ ]	70	80	-	-
Burner Exit Temperature [K]	1750	1900	1825	1725
Turbine Entry Temperature [K]	1706	1850	1773	1678
$\dot{m}$ [ $kgs^{-1}$ ]	708	792	250	164
$\dot{m}_{corr}$ [ $kgs^{-1}$ ]	759	867	1141	750
Propulsive Efficiency [%]	43.3	40.0	72.1	73.3
Core Efficiency [%]	50.1	51.1	57.9	57.6
$T_R$ per Engine [kN]	116	232	84	29.9
<b><math>T_A</math> per Engine [kN]</b>	<b>180.9</b>	<b>237.0</b>	<b>86.2</b>	<b>53.2</b>

## 7 Fan Design

The fan was designed to maximise angular velocity, limited by a maximum Mach number of the tip of 1.3. As discussed in Section 5.8, the tip diameter of the fan ( $D_{tip}$ ) is 2.6 m.

$$\Omega_{LP} = \frac{2U_{tip}}{D_{tip}} = \frac{2M\sqrt{\gamma RT_{fan}}}{D_{tip}} \quad (10)$$

Using Equation 10, the fan speed was determined to be 294.67 rad/s, equaling the LP compressor and LP turbine since they are connected via a single shaft.

The hub-to-tip (h) ratio was fixed at 0.35 [13] which combined with the tip diameter, fixed the hub diameter of the fan at 0.91 m. The inner fan was defined as the portion of the fan which compresses the air that enters the core. This is dictated by the bypass ratio (BPR) which was

7 [14]. The inner fan diameter of 0.325 m was calculated using Equation 11. The mean radius of the inner fan is halfway between the hub and inner fan diameter.

$$D_{inner\ fan} = \frac{(1 + BPR \times h^2)}{\sqrt{(1 + BPR)}} \quad (11)$$

It was decided the inner fan pressure ratio would match the outer fan pressure ratio which was set to 1.8 in Section 6.4. As such the engine would require a LP booster stage to achieve the necessary 2.5 pressure ratio before entering the HP compressor. Between the fan and the LP booster, inlet guide vanes would be needed to redirect the flow axially.

## 8 Compressor Design

The flow chart in Figure 9 outlines the process used to design the compressors.

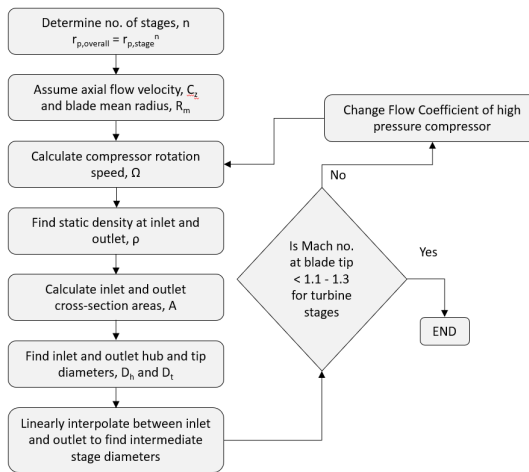


**Figure 9:** Flow chart detailing compressor design methodology.

### 8.1 Number of Stages

The pressure ratio of the LP booster was determined by dividing the pressure ratio across both the fan and the booster stages, 2.5 by the inner fan pressure ratio, 1.8. This yielded a booster pressure ratio of 1.39. Since the pressure ratio across each compressor stage should be less than 1.3 [13], at least 2 booster stages were required, resulting in a pressure ratio of 1.18 across both booster stages.

The number of stages,  $n$  in the HP compressor was calculated using Equation 12 where the total pressure ratio,  $r_{p,total}$  is the product of the pressure ratios of each stages,  $r_{p,stage}$ . The calculated  $n$  was rounded up to ensure sufficient pressure rise. The pressure ratio across the HP compressor was specified at 16 [14] and the pressure rise across each stage was set to the maximum permissible pressure rise of 1.3 [13], resulting in an 11 stages.

$$r_{p,total} = r_{p,stage}^n \quad (12)$$

### 8.2 Axial Velocity

The axial flow velocity ( $C_z$ ) through all compressor stages was fixed at 180 m/s [12].

### 8.3 Angular Velocity

The LP compressor rotates with the fan at an angular velocity of 294.7 rad/s.

The HP compressor rotates independently of the fan and LP compressor. The angular velocity was chosen so that the flow coefficient ( $\phi$ ) shown in Equation 25 was 0.5 [13]. The mean velocity ( $U_{mean}$ ) combined with the mean radius of the blade ( $r_{mean}$ ) means the HP compressor rotates at 600 rad/s as per Equation 23.

$$\phi = \frac{C_z}{U_{mean}} \quad (13)$$

### 8.4 Cross-Sectional Area

The stagnation density,  $\rho_0$  was calculated from the ideal gas equation (Equation 14) using the stagnation pressures and temperatures at the compressor inlet and outlet calculated by GasTurb (Appendix A.2).

$$\rho_0 = \frac{P_0}{RT_0} \quad (14)$$

Next, the static density was determined from Equation 15. The flow at the entry and exit of the compressors is primarily axial such that the Mach number in the equation can be substituted for the Mach number associated with the axial flow,  $M_z$ .

$$\rho = \frac{\rho_0}{(1 + (\frac{\gamma-1}{2})M_z^2)^{\frac{1}{\gamma-1}}} \quad (15)$$

The areas of the inlet and outlet of each compressor were calculated from Equation 16. The mass flow rate through the core was determined to be 20.5  $\frac{kg}{s}$  in Task 1 [14].

$$A = \frac{\dot{m}}{\rho C_z} \quad (16)$$

### 8.5 Low Pressure Diameters

It was decided that the mean radius of the LP compressor would match the mean radius of the inner fan as described in Section 7. A mean radius of 0.54 m was calculated and set as constant across the LP compressor. The hub diameter and tip diameter at the inlet and outlet of the LP turbine was calculated from the mean radius and the cross-sectional areas specified in Section 8.4 with Equations 17 and 18.

$$D_{tip} = \frac{4\pi r_{mean}^2 + A}{2\pi r_{mean}} \quad (17) \qquad \qquad D_{hub} = \frac{4\pi r_{mean}^2 - A}{2\pi r_{mean}} \quad (18)$$

The hub and tip diameters of the intermediary stages were then found by linear interpolation between the inlet diameter and outlet diameter of the compressors.

### 8.6 High Pressure Diameters

The smallest blade length in the compressor ( $L_b$ ) must exceed 10 mm [13]. The smallest blade in the high pressure compressor is the final blade whose length was conservatively set to 12 mm.

The hub and tip diameters at exit were calculated using Equations 19, 20 and the exit area calculated in Section 8.4.

$$D_{hub} = \frac{(A - \pi L_b^2)}{\pi L_b} \quad (19)$$

$$D_{tip} = D_{hub} + 2L_b \quad (20)$$

$$R_{mean} = \frac{D_t + D_h}{4} \quad (21)$$

The mean radius of the compressor blades was half way between these diameters (Equation 21). It was decided that the mean radius would be constant for all stages.

The hub and tip diameters at the inlet of the HP compressor were calculated from this compressor mean radius and the area of the inlet found in Section 8.4 using Equations 17 and 18 in the same way as for the LP compressor. The hub and tip diameters of the intermediary stages were found by linear interpolation between the inlet diameter and outlet diameter of the compressors.

## 8.7 Validation

The Mach number at the blade tips could not exceed 1.1-1.3. Verifying this for the LP booster stages is unnecessary given it shares the same angular velocity as the fan, which has been designed for the worst case of 1.3 Mach number at the fan tip. Hence the blade tip mach number of the LP boosters will always be less than 1.3. Furthermore verifying this for the HP compressor is also unnecessary given the blade tip mach number of the turbine will always be the limiting factor. This is a consequence of the higher temperatures experienced by the turbine, the larger mean radius and the fact that the maximum tip diameter of the turbine exceeds that of the compressor. Hence blade tip mach number is not verified for the compressors but instead, only for the turbine.

## 8.8 Compressor Summary

**Table 6:** LP Compressor Stage Values

Stage	Fan	1	2
$D_t$ [m]	2.600	1.124	1.119
$D_h$ [m]	0.910	1.038	1.043
$L_b$ [mm]	845.0	42.98	37.80
$r_{p,stage}$	1.8	1.18	1.18

**Table 7:** HP Compressor Stage Values

Stage	1	2	3	4	5	6	7	8	9	10	11
$D_t$ [m]	0.5412	0.5333	0.5254	0.5175	0.5096	0.50167	0.4938	0.4859	0.4780	0.4701	0.4622
$D_h$ [m]	0.3592	0.3671	0.3750	0.3829	0.3908	0.3987	0.4066	0.4145	0.4223	0.4303	0.4318
$L_b$ [mm]	90.96	83.07	75.17	67.28	59.38	51.48	43.58	35.69	27.79	19.89	12.00
$r_{p,stage}$	1.3	1.3	1.3	1.3	1.3	1.3	1.3	1.3	1.3	1.3	1.3

## 9 Turbine Design

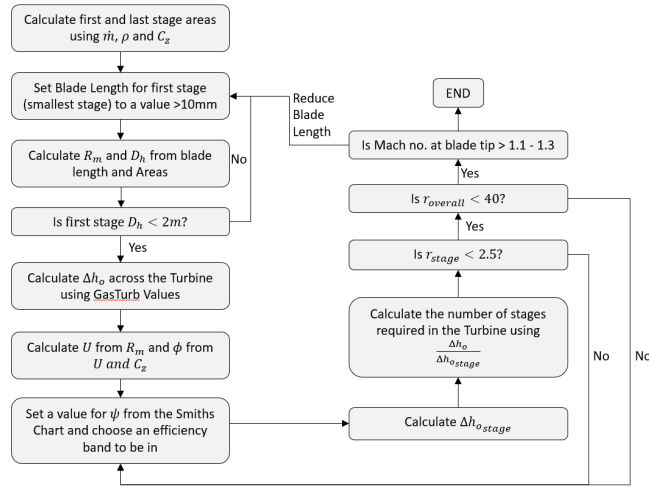


**Figure 10:** Flow chart detailing turbine design methodology.

### 9.1 Axial Velocity

The axial flow through all turbine stages was fixed at 150 m/s [4].

### 9.2 Angular Velocity

The angular velocity ( $\Omega$ ) of the LP turbine was fixed to the LP compressor ( $294.67 \text{ rads}^{-1}$ ) and the HP turbine was fixed to the HP compressor ( $850 \text{ rads}^{-1}$ ) as shown in Section 8.3.

### 9.3 Cross Sectional Area

The area of the entry of the turbine and the exit of the turbine were calculated from the thermodynamic properties from GasTurb in Task 1 [14]. This is the same process as was used for the compressors in Section 8.4.

### 9.4 Diameters

The first blade length of both the HP and LP turbines was calculated to be 23 mm and 31 mm respectively, far above the minimum practical blade length of 10 mm[13]. Using Equations 19, 20 and the areas calculated in Section 9.3, the inlet hub and tip diameters were calculated. The mean radius was calculated using Equation 21 and assumed to be constant throughout all stages in the turbine. The outlet hub and tip diameters were calculated from the cross-sectional area of the outlet and the mean radius in the same way as the LP compressor in Section 8.5 using Equations 17 and 18. The diameters of each of the intermediate stages were linearly interpolated from the inlet and outlet diameters.

The blade lengths for each of the stages were calculated using Equation 22.

$$L_b = \frac{D_t - D_h}{2} \quad (22)$$

The mean velocity of the blades was calculated using Equation 23. Note that it is constant due to the constant angular velocity and mean radius.

$$U_m = \Omega R_m \quad (23)$$

## 9.5 Number of Stages

The work produced by the HP turbine must be equal to the work needed to drive the HP compressor which is related to the change in stagnation enthalpy ( $\Delta h_0$ ) across the turbine as shown in Equation 24 where  $T_{01}$  and  $T_{02}$  are the entry and exit stagnation temperatures of the turbine which were found in Task 1 [14].

$$\Delta h_0 = C_p(T_{02} - T_{01}) \quad (24)$$

The flow ( $\Phi$ ) and work ( $\Psi$ ) coefficients were calculated using Equations 25 and 26 respectively.

$$\Phi = \frac{C_z}{U} \quad (25)$$

$$\Psi = \frac{\Delta h_{0,stage}}{U^2} \quad (26)$$

A target turbine efficiency was selected and the corresponding work coefficient,  $\Psi$  value was identified using the Smith chart in Figure 11. The final values were  $\Psi = 2.6$  and  $\Phi = 0.78$  for the LP turbine and  $\Psi = 1.8$  and  $\Phi = 0.54$  for the HP turbine which correspond to a total to total efficiency of 87% and 89% respectively.

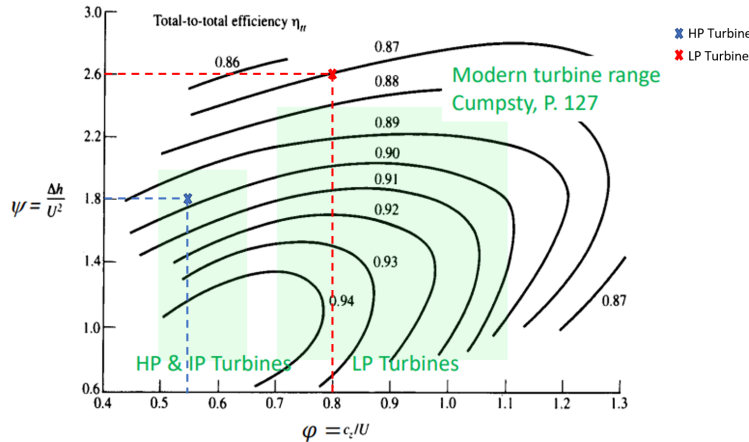


**Figure 11:** Smith Chart showing efficiency contours with respect to work coefficient ( $\Psi$ ) and flow coefficient ( $\Phi$ ) [4]

$\Psi$  was used to calculate the change in stagnation enthalpy per stage of the turbine by rearranging Equation 26. The change in stagnation enthalpy was constant across all stages of each turbine, since  $\Psi$  and  $U$  were constant across all stages.

The number of stages within each turbine was calculated using Equation 27.

$$n = \frac{\Delta h_0}{\Delta h_{0,stage}} \quad (27)$$

The HP turbine had 3 stages and the LP turbine had 4 stages. If the HPT had any fewer stages the pressure ratio across each stage would exceed the 2.5 maximum.

## 9.6 Design Validation

Checks were performed to ensure that the pressure ratio per stage could not exceed 2.5 for any turbine stage. Also the combined pressure ratio of all of the HP and LP turbines stages could not exceed 40 to prevent the air from being over-expanded, generating losses. Finally, the Mach number of the blade tips could not exceed 1.1-1.3 [12] to minimise losses.

### 9.6.1 Pressure Ratio Validation

The entropy change across any stage within the turbine is constant thus the change in temperature is also constant as per Equation 28.

$$\Delta T_{0stage} = \frac{1}{C_p} \Delta h_{0stage} \quad (28)$$

The pressure ratio across each of the stages was calculated using Equation 29 with an isentropic efficiency of 0.92 [14], such that the pressure ratio across each stage was less than 2.5, verifying that the maximum pressure drop criteria was met (Table 14a and 14b).

$$r_{p,stage} = \left(1 - \frac{\Delta T_{0,stage}}{\eta_s T_{01,stage}}\right)^{\frac{\gamma}{1-\gamma}} \quad (29)$$

### 9.6.2 Combined Pressure Ratio Validation

The thermodynamic cycle detailed in Task 1 required a combined pressure ratio of 40 through both the HP and LP turbine. This is to mirror the pressure ratio of the LP and HP compressors and also so that the static pressure of the air leaving the turbine is atmospheric. With the specified geometry, the current turbines have a combined pressure ratio of 37.9 such that the exit static pressure will be slightly higher than atmospheric. This was deemed better than alternative which results in an adverse pressure gradient that would accelerate the flow in the direction that counteracts thrust generated.

### 9.6.3 Tip Mach Number Validation

The tip velocity is different for each blade as the blade length vary. They were calculated using Equation 30 and all were below Mach 1.3 (Table 14a and 14b).

$$M = \frac{U_{tip}}{c} = \frac{l\Omega}{\sqrt{\gamma RT}} \quad (30)$$

## 9.7 Turbine Summary

**Table 8:** HP Turbine Stage Values

Stage	1	2	3
$D_t$ [m]	0.672	0.691	0.710
$D_h$ [m]	0.626	0.608	0.589
$L_b$ [mm]	22.99	41.85	60.70
$r_{p,stage}$	1.682	1.773	1.890
$M_{tip}$	0.349	0.384	0.425

**Table 9:** LP Turbine Stage Values

Stage	1	2	3	4
$D_t$ [m]	1.330	1.355	1.380	1.406
$D_h$ [m]	1.268	1.242	1.217	1.192
$L_b$ [mm]	30.99	56.38	81.76	107.12
$r_{p,stage}$	1.512	1.569	1.639	1.729
$M_{tip}$	0.276	0.296	0.319	0.348

## 10 Compressor Blade Design

### 10.1 Blade Angles

The blade angles at the mean radius for each stage of the compressors were calculated using the Euler Equation (31) and the Reaction Equation (32) for compressors in the relative reference frame.

$$\Lambda = \frac{C_z}{2U}(\tan(\beta_1) + \tan(\beta_2)) \quad (31) \quad \Psi = \frac{C_z}{U}(\tan(\beta_1) - \tan(\beta_2)) \quad (32)$$

These equations were rearranged to solve for the beta values in Equation 33 and Equation 34. Note that while deriving the equations, the beta values were drawn to be in the direction opposite to the direction of rotation, hence why the output from Equations 33 and 34 was expected to be positive.

$$\beta_1 = \tan^{-1}\left(\frac{2\Lambda + \Psi}{2\Phi}\right) \quad (33) \quad \beta_2 = \tan^{-1}\left(\frac{2\Lambda - \Psi}{2\Phi}\right) \quad (34)$$

The beta values were then converted to alpha values using the velocity triangles to produce Equations 35 and 36.

$$\alpha_1 = \tan^{-1}\left(\frac{U}{C_z} - \frac{2\Lambda + \Psi}{2\Phi}\right) \quad (35) \quad \alpha_2 = \tan^{-1}\left(\frac{U}{C_z} - \frac{2\Lambda - \Psi}{2\Phi}\right) \quad (36)$$

The outlet flow from the fan into the first stage of the LP compressor was assumed to be fully axial. Thus inlet guide vanes were added to turn the flow to the required angle. The outlet of the HP compressor was axial.

The blade angles at the hub radius and tip radius were calculated from the mean angles using the assumption of radial equilibrium ( $rC_\theta = constant$ ). Equation 37 relates the the velocity of the flow at different radii.

$$r_{mean}C_{\theta mean} = r_{hub}C_{\theta hub} = r_{tip}C_{\theta tip} \quad (37)$$

Using the velocity triangles of the flow, the alpha values at the hub and tip were calculated from the alpha values at the mean radius using Equations 38 and 39. This allowed the blade angles at each radial step to be found which are illustrated for the first LPC stage in the cross-sectional drawings in Figure 12, with each radial step overlaid in Figure 22a in Appendix A.3.

$$\alpha_{tip} = \tan^{-1}\left(\left(\frac{r_{mean}}{r_{tip}}\right)\tan(\alpha_{mean})\right) \quad (38) \quad \alpha_{hub} = \tan^{-1}\left(\left(\frac{r_{mean}}{r_{hub}}\right)\tan(\alpha_{mean})\right) \quad (39)$$

### 10.2 Solidity

The solidity of each turbine stage was calculated from Equation 40 where the Diffusion factor ( $D_F$ ) has a maximum value of 0.45.

$$D_F = 1 - \frac{C_2}{C_1} + \frac{1}{2} \frac{C_{\theta 2} - C_{\theta 1}}{C_1} \frac{s}{c} \quad (40)$$

Using the velocity triangles for the turbine, Equation 40 was rearranged into Equation 41. Solidity had to be between 0.67 and 1.33 to be considered valid [4].

$$\sigma = \frac{(tan\alpha_2 - tan\alpha_1)cos\alpha_1cos\alpha_2}{2((D - 1)cos\alpha_2 + cos\alpha_1)} \quad (41)$$

### 10.3 Number of Blades

The number of blades for each compressor stage was calculated using Equation 42 using the solidity and the aspect ratio ( $\frac{h}{c}$ ). The aspect ratio for both the HPC and LPC rotor and stator stages was set at 1.75 which is half-way between the typical range of 1 - 2.5 suggested by literature [15] [4].

$$n_{rotor} = \frac{2\pi r_{mean}\sigma \frac{h}{c}}{h} \quad (42)$$

The number of blades in the stator was one less than the number of blades in the rotor. This was to ensure that the stator rotor blade number ratio remained as high as possible, to reduce the flow non uniformity and blade oscillations [16].

### 10.4 Aerodynamic Validation

The blades and angles were checked against aerodynamic criteria to determine if they were suitable. The final values, given in Section 10.5, met all these criteria.

- The tip of the blade less than  $M=1.3$ .
- The blade length greater than 10mm.
- $|\beta_2| < |\beta_1|$
- $\beta_1 - \beta_2 < 45^\circ$
- $0.67 < \sigma < 1.3$
- $D_F < 0.5$

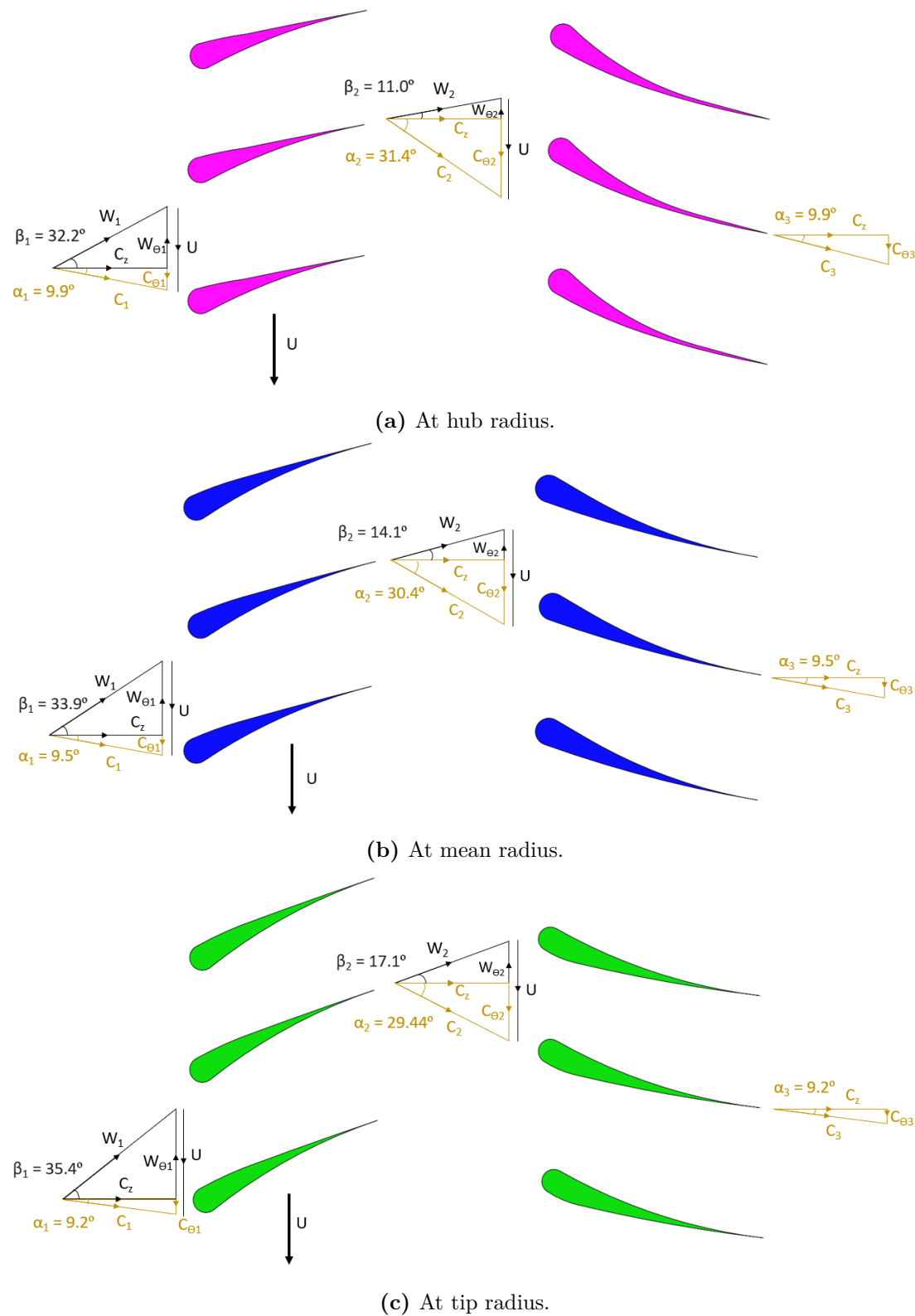


**Figure 12:** Cross-sectional drawing in the axial-tangential plane of the blades in the inlet LPC stage. These are illustrated at 3 different radial heights corresponding to the hub (12a), mean (12b) and tip (12c) radii. Flow velocity triangles are overlaid to indicate flow deflection through the stage.

## 10.5 Summary

Tables 10 - 12 summarise the key values for each stage of the compressors.

**Table 10:** Blade angles and solidity ( $\sigma$ ) at mean radius of all stages of the low (10a) and high (10b) pressure compressors.

(a) LPC		(b) HPC	
	Repeating Stages		Repeating Stages
$\alpha_1$ [°]	9.52	$\alpha_1$ [°]	1.44
$\alpha_2$ [°]	30.41	$\alpha_2$ [°]	27.86
$\beta_1$ [°]	-33.85	$\beta_1$ [°]	-44.47
$\beta_2$ [°]	-14.12	$\beta_2$ [°]	-25.57
$\sigma$	0.872	$\sigma$	0.847

**Table 11:** Number of blades in the stator and rotor of each stage in the low (11a) and high (11b) pressure compressors.

(a) LPC		(b) HPC												
Stage	1	2	Stage	1	2	3	4	5	6	7	8	9	10	11
$n_{rotor}$	121	137	$n_{rotor}$	23	25	28	31	35	41	48	59	75	105	175
$n_{stator}$	120	136	$n_{stator}$	22	24	27	30	34	40	47	58	74	104	174

**Table 12:** Blade angles, reaction ( $\Lambda$ ), diffusion factor ( $D_F$ ), work coefficient ( $\Psi$ ) and flow coefficient ( $\Phi$ ) at hub, mean and tip radii for the first stage of the low (12a) and high (12b) pressure compressors

(a) LPC				(b) HPC			
Radius	Hub	Mean	Tip	Radius	Hub	Mean	Tip
$\alpha_1$ [°]	9.91	9.52	9.16	$\alpha_1$ [°]	1.81	1.44	1.20
$\alpha_2$ [°]	31.44	30.41	29.45	$\alpha_2$ [°]	33.53	27.86	23.74
$\beta_1$ [°]	-32.23	-33.85	-35.40	$\beta_1$ [°]	-37.67	-44.47	-49.95
$\beta_2$ [°]	-10.97	-14.12	-17.08	$\beta_2$ [°]	-8.02	-25.56	-37.62
$\Lambda$	0.512	0.550	0.584	$\Lambda$	0.57	0.725	0.81
$\Psi$	0.542	0.500	0.462	$\Psi$	0.785	0.500	0.346
$\Phi$	1.242	1.192	1.147	$\Phi$	1.24	0.99	0.83
$D_F$	0.099	0.100	0.100	$D_F$	0.173	0.167	0.155

## 11 Turbine Blade Design

The blade angles at the mean radius for each stage of the turbine were calculated using the Euler Equation 43 and the Reaction Equation 44 for turbines in the relative reference frame.

$$\Lambda = -\frac{C_z}{2U}(\tan(\beta_3) + \tan(\beta_2)) \quad (43)$$

$$\Psi = \frac{C_z}{U}(\tan(\beta_2) - \tan(\beta_3)) \quad (44)$$

These equations were rearranged to solve for the beta values in Equation 45 and Equation 46.

$$\beta_2 = \tan^{-1}\left(-\frac{2\Lambda - \Psi}{2\Phi}\right) \quad (45)$$

$$\beta_3 = \tan^{-1}\left(-\frac{2\Lambda + \Psi}{2\Phi}\right) \quad (46)$$

The beta values were then converted to alpha values using Equations 47 and 48.

$$\alpha_2 = \tan^{-1}\left(\frac{U}{C_z} - \frac{2\Lambda - \Psi}{2\Phi}\right) \quad (47)$$

$$\alpha_3 = \tan^{-1}\left(\frac{U}{C_z} - \frac{2\Lambda + \Psi}{2\Phi}\right) \quad (48)$$

The flow exiting the combustor and then entering the first stage of the HP turbine was assumed to be fully axial. The exit of the final stage of the LP turbine was also set to be fully axial. However the outputs of intermediate stages were not fully axial.

The blade angles at the hub radius and tip radius were calculated in the same way as the compressor from the mean angles using the assumption of radial equilibrium ( $rC_\theta = \text{constant}$ ). Equation 49 relates the the velocity of the flow at different radii.

$$r_{mean}C_{\theta mean} = r_{hub}C_{\theta hub} = r_{tip}C_{\theta tip} \quad (49)$$

Using the velocity triangles of the flow, the hub and tip alpha values were calculated from the alpha values at the mean radius using Equations 38 and 39. The angles derived at the hub, mean and tip radii define the blade profile at these radial stages. These are illustrated in the cross-sectional drawings in Figure 13 for the first stage of the HPT, each of which are overlaid in Figure 22b in Appendix A.3.

## 11.1 Solidity

The solidity of the turbine was calculated from Equation 50. An initial starting value of lift coefficient,  $C_L = 0.8$ , known as Zweifel's criterion [15] was used. This value was allowed to vary during the iterative calcualtion process but it was ensured that the final values of  $C_L$  were close to 0.8, to ensure the best compromise between number of blades and flow guidance [4][15].

$$C_L = 2\frac{s}{c}\cos^2(\alpha_2)(\tan\alpha_1 - \tan\alpha_2) \quad (50)$$

When rearranged, the solidity is a function of blade angles and the lift coefficient as in Equation 51. Solidity must be between 1 and 2 to be considered valid.

$$\sigma = \frac{c}{s} = \frac{2\cos^2(\alpha_1)(\tan(\alpha_1) - \tan(\alpha_2))}{C_L} \quad (51)$$

## 11.2 Number of Blades

The number of blades was calculated in the same way as for the compressor using Equation 42 which is a function of the solidity and the aspect ratio ( $\frac{h}{c}$ ). The number of stator blades was

reduced by one for the turbines as explained previously for the compressor. The aspect ratio for the turbines was set to be the middle values in the typical ranges suggested by literature [4] [15] and are given in Table 13.

**Table 13:** Blade aspect ratios ( $\frac{h}{c}$ ) for turbine stages.

$\frac{h}{c}$	HPT	LPT
Rotor	2.5	3
Stator	1.5	2.5

### 11.3 Aerodynamic Validation

The blades and angles were checked against aerodynamic criteria to determine if they were suitable. The final values, given in Section 11.4, met all these criteria.

- The tip of the blade less than  $M=1.3$ .
- The blade length greater than 10mm.
- $100^\circ < \varepsilon$  (flow deflection)  $< 120^\circ$
- Reaction ( $\Lambda$ )  $> 0$  at the hub.
- Reaction ( $\Lambda$ )  $< 1$  at the tip.

### 11.4 Summary

Tables 14 - 16 summarise the key values for each stage of the turbines.

**Table 14:** Blade angles and solidity,  $\sigma$  in each stage of the high (14a) and low (14b) pressure turbines.

(a) HPT		(b) LPT	
	Repeating Stages		Repeating Stages
$\alpha_2$	68.80	$\alpha_2$	66.47
$\alpha_3$	-36.38	$\alpha_3$	-45.58
$\beta_2$	36.38	$\beta_2$	45.58
$\beta_3$	-68.80	$\beta_3$	-66.47
$\sigma$	1.08	$\sigma$	1.24

**Table 15:** Number of blades for the rotor and stator in each stage of the high (15a) and low (15b) pressure turbines.

(a) HPT		(b) LPT						
Stage	1	2	3	Stage	1	2	3	4
$n_{rotor}$	240	132	91	$n_{rotor}$	491	270	186	142
$n_{stator}$	239	131	90	$n_{stator}$	490	269	185	141

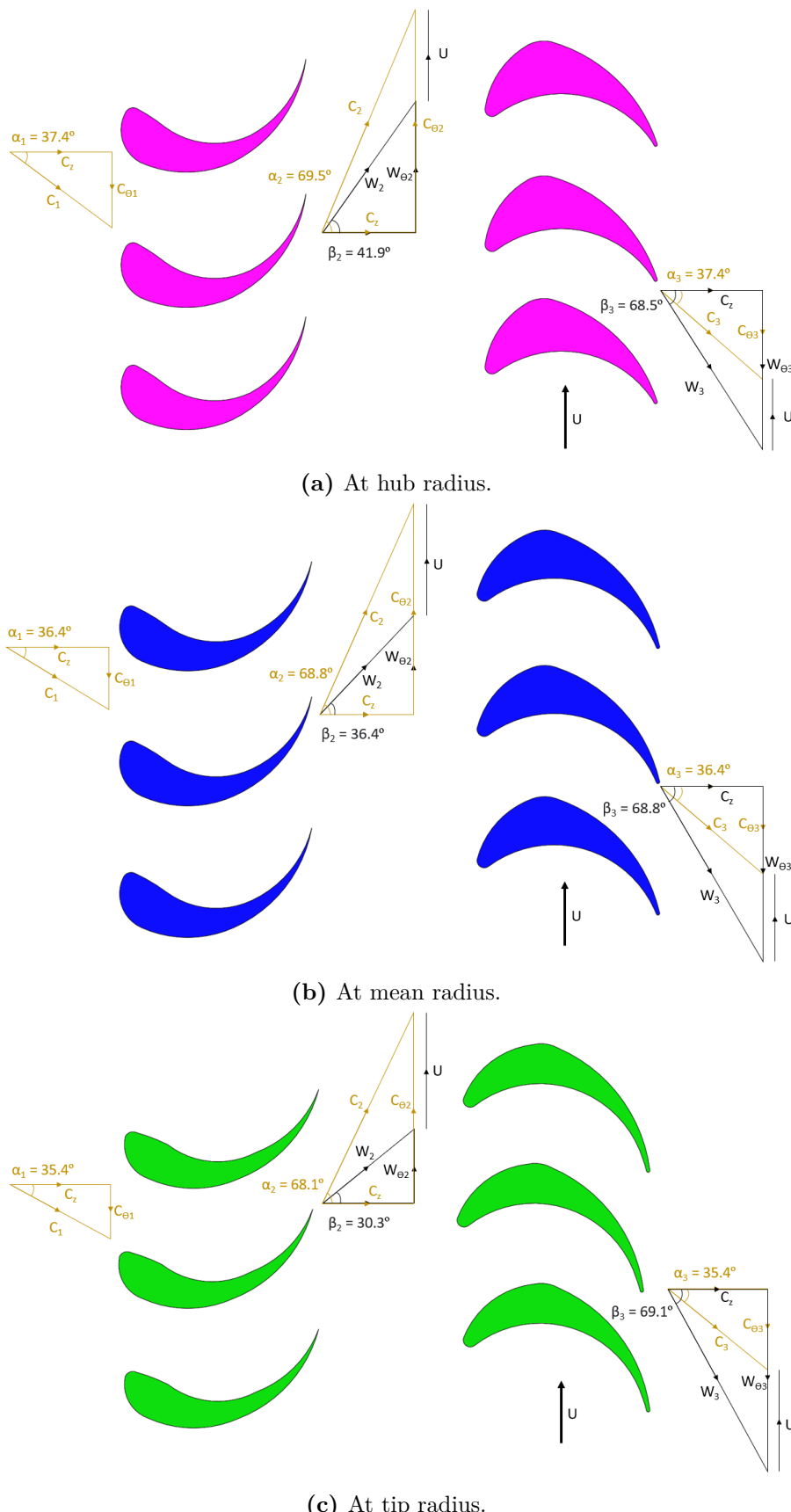


**Figure 13:** Cross-sectional drawing in the axial-tangential plane of the blades in the 1st HPT stage. These are illustrated at 3 different radial heights corresponding to the hub (13a), mean (13b) and tip (13c) radii. Flow velocity triangles are overlaid to indicate flow deflection through the stage.

**Table 16:** Blade angles, reaction ( $\Lambda$ ), work coefficient ( $\Psi$ ), flow coefficient ( $\Phi$ ) and lift coefficient ( $C_L$ ) at hub, mean and tip radii for the first stage of the low (16a) and high (16b) pressure turbines.

(a) LPT				(b) HPT			
Radius	Hub	Mean	Tip	Radius	Hub	Mean	Tip
$\alpha_2$	66.97	66.47	65.97	$\alpha_2$	69.49	68.80	68.12
$\alpha_3$	-46.27	-45.58	-44.91	$\alpha_3$	-37.37	-36.38	-35.43
$\beta_2$	47.91	45.58	43.12	$\beta_2$	41.87	36.38	30.25
$\beta_3$	-66.42	-66.47	-69.09	$\beta_3$	-68.51	-68.80	-66.53
$\varepsilon$	114.33	112.05	112.21	$\varepsilon$	110.38	105.18	96.78
$\Lambda$	0.48	0.50	0.52	$\Lambda$	0.46	0.50	0.53
$\psi$	2.73	2.6	2.48	$\psi$	1.93	1.8	1.68
$\phi$	0.80	0.78	0.77	$\phi$	0.56	0.54	0.52
$C_L$	0.84	0.85	0.86	$C_L$	0.77	0.8	0.82

## 12 Parameter Optimisation Algorithm

A bespoke python package was developed to design and analyse 2-spool turbo-fan engines. It includes methods for calculating engine performance, geometry, and thermodynamic properties. The package also includes tools for optimising engine designs and visualizing engine components and results.

### 12.1 Software Architecture

There are numerous requirements for an engine to be functional. Changing a single input parameter can have cascading effects on the output values. The effect of changing one such parameter can be analytically found. However, with multiple parameters to vary, the challenge of predicting the effect on outputs multiplies.

To simplify the design process, the code was abstracted in an object-oriented manner into base classes representing each component, as shown in Figure 23. Each sub-class has their own functions and properties relating solely to that component.

Subsequently, any property of a desired component could be accessed directly from the parent `Engine` object after running the program with a set of initial conditions. All properties of the `Engine` object and its sub-components for the final design can be found in Appendix A.7.

### 12.2 Optimising Iterator

A rigorous multi-variable optimisation iterator was developed to help identify the optimal input parameters to get a desired engine output. A desired engine design not only meets the set out criteria, but the parameters are in the optimal in the ranges specified.

The iterator (coded in Python, with the link to the GitHub repository available in Appendix A.5), worked on the concept of sweeping through every possible combination in the variable ranges with a specified step size and as such tested over two million possible design cases.

The following variables were varied across ranges, with most of the ranges coming from literature, and the rest being engineering estimates. Fewer or more variables could be varied, but these were selected as other variables would change design parameters already selected in previous tasks.

**Table 17:** Input parameter sweep ranges varied with the iterator.

Parameters	Range
LPC Diffusion Factor	$0.2 < D < 0.5$
HPC Diffusion Factor	$0.2 < D < 0.5$
LPT Lift Coefficient	$0.7 < C_L < 1$
HPT Lift Coefficient	$0.7 < C_L < 1$
LPC Reaction	$0.5 < \Lambda < 0.9$
HPC Reaction	$0.5 < \Lambda < 0.9$
HPT Work Coefficient	$0.8 < \Psi < 2$
HPT Angular Velocity	$500 < \omega < 1500$
HPT Min Blade Length	$0.012 < L_b < 0.03$

To pass the checks and be an "approved" engine design, the designs were run past a criteria checking loop, where the working conditions of the engine was compared against specific criteria to narrow down the possible engine designs. These criteria were given in Section 10.4 for the compressors and Section 11.3 for the turbines.

Additionally, a secondary iteration used the "valid" engine designs from the first iteration and repeated the optimization for a narrowed range. The refined range was defined by the range of each variable from the already "valid" engines. This helped refine the optimization even more, which in turn increased the number of "valid" engines.

To select one engine from the set of "valid" engines, a scoring algorithm was developed to rank the suitability of each engine. The scoring system rewarded points for parameter within the known desired range and penalised engines where parameters deviated. This was done using a rising or falling smoothed step function of a certain height to simulate the relative importance of that parameter.

Over a million different combinations for the first iteration, with the number rising over to 20 million in the second iteration. From there, there were approximately 100,000 successful engines, which were then ranked using the scoring system. The final engine was had the best combination of properties. All of the equations used for the optimization process are described in the relevant sections of this report.

## 13 Stress Analysis

### 13.1 Disk Stress

The blade disks were analysed to determine their safety factor against yielding.

#### 13.1.1 Assumptions

The following assumptions were used through the calculations.

1. The disk is made from Inconel 718 (IN718) which has a density of  $8,193.25 \frac{kg}{m^3}$  and a Poisson's ratio of 0.27. [17]
2. The disks are assumed to be thin enough for axial stresses to be negligible.
3. The disk has a constant thickness. This will be re-evaluated in Section 13.2
4. There is a uniform temperature across the disk so stresses caused by temperature are negligible.
5. The deformation is purely in the elastic region of the material.
6. The disk is a solid body so it rotates with a constant angular velocity.

### 13.1.2 Radial and Hoop Stress

The radial stress and hoop stress in a disk of constant thickness were calculated from Equations 52 and 53 [18] respectively.

$$\sigma_r = \frac{3 + \nu}{8} \rho \Omega^2 (R_i^2 + R_o^2 - \frac{R_i^2 R_o^2}{r^2} - r^2) + \frac{N_b F_{rim} R_o}{2\pi h (R_o^2 - R_i^2)} (1 - (\frac{R_i}{r})^2) \quad (52)$$

$$\sigma_\theta = \frac{3 + \nu}{8} \rho \Omega^2 (R_i^2 + R_o^2 + \frac{R_i^2 R_o^2}{r^2} - \frac{(1 + 3\nu)}{3 + \nu} r^2) + \frac{N_b F_{rim} R_o}{2\pi h (R_o^2 - R_i^2)} (1 + (\frac{R_i}{r})^2) \quad (53)$$

$F_{rim}$  is the force on the rim of the disk caused by the attached mass of the blade. It was calculated using Equation 62 which is derived in Appendix A.4. The thickness of the blade ( $t$ ) is taken to be 15% of the chord length ( $c$ ).

$$F_{rim} = \Omega^2 \rho c t L_{blade} (R_i + \frac{L_{blade}}{2}) \quad (54)$$

The stress distributions within the first disk of the high pressure turbine are shown in Figure 14. This is the disk with the highest stresses.

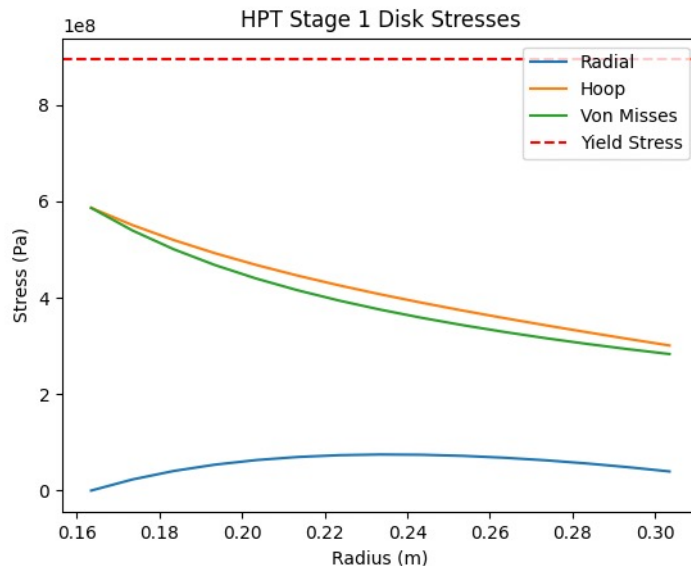


**Figure 14:** Radial, Hoop and Von-Mises Stress distributions across the radius of the disk of the first stage of the HPT

### 13.1.3 Safety Factors

With the radial and hoop stresses in the disk determined, the Von-Mises yield criteria was used to determine the equivalent stress (Equation 55) to compare to the yield stress found in literature. The stress axially through the disk ( $\sigma_z$ ) was assumed to be negligible compared to the radial and hoop stress.

$$\sigma_{VonMisesEquivalent} = \frac{1}{\sqrt{2}}((\sigma_z - \sigma_\theta)^2 + (\sigma_\theta - \sigma_r)^2 + (\sigma_r - \sigma_z)^2)^{\frac{1}{2}} \quad (55)$$

The prescribed material of the turbine disc is Inconel 718 (IN718) [19] whose yield stress varies with temperature according to the trend in Figure 15. Despite the entry conditions of the air at the entry of the turbine having a high temperature, cooling from the air siphoned off from the exit of the HP compressor will cool the turbine blades. Therefore, the blade disk surface temperature at the HPT inlet blade will be much lower than the air temperature coming out of the combustor, quoted from literature at 650°C [20]. The blade surface temperature at subsequent stages in the HPT was calculated by subtracting the change in static temperature from stage-to-stage (found from the isentropic flow relations) from the 650°C starting value. These values were used to find the yield stress of IN718 at the temperature of each stage.

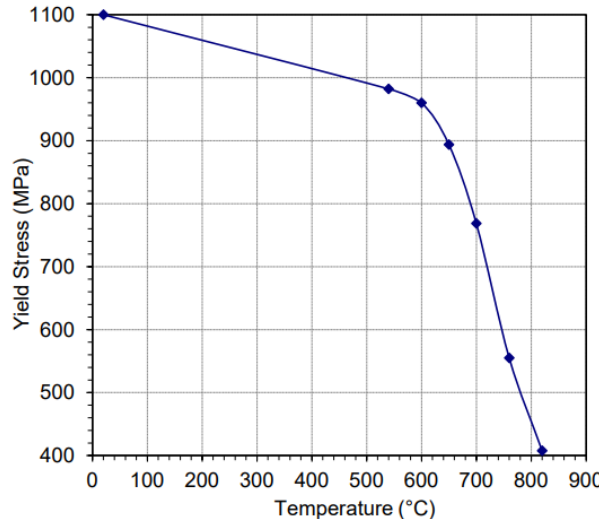


**Figure 15:** Graph showing the variation in yield stress with temperature for IN718 [21].

The Von-Mises equivalent stress and the yield stress was used to find the safety factor of the disk of each stage.

$$SF = \frac{\sigma_{yield}}{\sigma_{VonMisesEquivalent}} \quad (56)$$

The safety factors for the three stages were 1.52, 1.60 and 1.58 which were deemed acceptable.

## 13.2 Optimum Thickness

In Section 13.1, the disk was assumed to have a constant thickness. However, this results in unnecessary weight and therefore the thickness of the disk will be optimised in this section. A disk with optimum shape is one with a uniform equivalent stress at ever point  $\sigma_r = \sigma_\theta = \sigma_0$ . When this criteria is fulfilled, thickness of the disk varies with radius according to Equation 58 where  $h_0$  is the thickness which was used to calculate  $\sigma_0$ .

$$h = h_0 e^{B(R_o^2 - r^2)} \quad (57)$$

$$B = \frac{\rho \Omega^2}{2\sigma_0} \quad (58)$$

This equation resulted in the optimal thickness distribution shown in Figure 16.

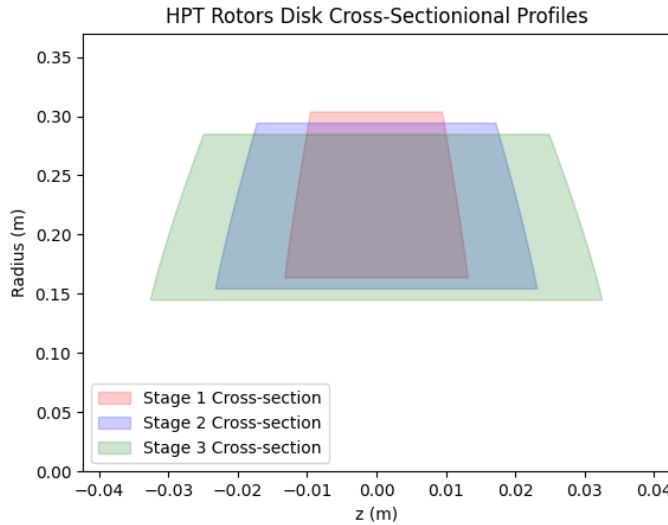


**Figure 16:** Optimum thickness distributions across the radius of the HPT rotor disk

## 14 Further Development

### 14.1 Turbine Mean Radius Assumption

In order to simplify calculations, the mean blade radius was assumed constant for all turbomachine stages. Whilst this assumption is commonly employed in the design of compressor stages, turbine stages are typically subject to different design conditions such as having a constant hub radius. Re-deriving engine sizing equations associated with the HPT and LPT using the constant hub radius assumption would, whilst complicating the underlying mathematics, lead to a more realistic final engine design.

### 14.2 Stress Analysis Assumptions

More detailed stress analysis are required for the disk and blades as the calculation in Section 13 are just estimates. The complex geometry of the disk and blades requires the use of Finite Element Analysis to accurately determine the stresses experienced during operation. Additionally, the temperature in the disk is not constant. Rather, there will be high temperature gradients, particularly during startup which will cause significant thermal stresses.

Along with failure due to exceeding the yield stress, failure due to fatigue and creep should be considered before certifying the design of the blade disks. This cyclic loading would be caused by the mechanical stress of starting and stopping the turbomachines spinning; vibration induced stresses caused by out of balance blades and disks; and by the thermal cycling, particularly on the surface of the turbine.

### 14.3 Work and Flow Coefficients

The values of work and flow coefficients of some of the turbomachines are not in their optimum ranges, as set out by Cumpsty [4] and is an area of the analysis which needs to be looked through more in the future. For example, the  $\psi$  value for the LP Turbine is beyond the limit of 2 [4], and the  $\phi$  value of the HP Compressor is beyond the limit of 0.75 [4]. This is due to the fact the parameter list for the iterator is so large and that the work and flow coefficients are all dependant on the variables (either directly or indirectly) such that changing the ranges chosen in Section 12 requires a lot of computational time, which was not possible during the timeframe.

## 15 Conclusion

The engine designed in this report fulfills the requirements for use in *The Air Tanker* and will provide the thrust needed to transport 30 tonnes of water from a local airport to an Australian bushfire 1500km away and returning safely. *The Air Tanker* utilises two of these, medium-bypass, two-spool, unmixed Turbofan engines.

The engines were optimised for a low Specific Fuel Consumption (*SFC*) and a high Specific Thrust ( $\frac{T}{m}$ ) at cruise but are also fairly efficient under cruise conditions, reaching core and propulsive efficiencies of 57.6% and 73.3% respectively. The engines each have a diameter of 2.6m with a bypass ratio of 7 and produce a thrust of 53.2 kN at cruise from a mass flow rate through the core of just 20.5 kg/s.

They can also provide the required thrust at take-off, top of climb and the case of single engine failure during take-off. The engines can each deliver a maximum thrust of 237.0 kN under take-off conditions without surpassing material temperature limits.

A fan, compressors and turbines were designed for use in this engine. The low pressure compressor was composed of the inner fan and two low pressure booster stages. The inner fan pressure ratio was 1.8 and each booster stage had a pressure ratio of 1.18, giving a total pressure ratio of 2.5. The low pressure system spun at an angular velocity of  $294.67 \text{ rads}^{-1}$ . The high pressure compressor was designed with 11 stages, each with a pressure ratio of 1.3 and spinning at  $850 \text{ rads}^{-1}$ . These were powered by the high pressure turbine which had 3 stages and an overall pressure ratio of 5.63, in conjunction with the low pressure turbine which had 4 stages, with an overall pressure ratio of 6.73. The maximum pressure ratio across a single stage was 1.89, far below the maximum pressure ratio limitation of 2.5. These parameters produced a design with a total-to-total efficiency of 89% for the high pressure turbine and 87% for the low pressure turbine at cruise. Furthermore, none of the Mach numbers in the tips exceeded the limitation for all the turbo machines.

The blade angles for the compressors and turbines were designed to maximize efficiency. Along with the angles at the mean radius, the blade angles at the hub and tip were calculated for one turbine stage and one compressor stage. These blades and angles passed the aerodynamic limit verification checks.

Finally, the stresses in the high pressure turbine disks were analyzed and determined to have a minimum safety factor of 1.52. The thickness of the disk was optimised so that unnecessary mass was removed.

## References

- [1] USDA. Fire management planes. URL <https://www.fs.usda.gov/managing-land/fire/planes>. [Accessed on 15th Jan 2023].
- [2] California Department of Forestry and Fire Protection. Firefighting aircraft recognition guide. <https://gacc.nifc.gov/swcc/dc/azpdc/operations/documents/aircraft/links/Aircraft%20Recognition%20Guide.pdf>. [Accessed on 15th Jan 2023].
- [3] R. Martinez-Botas. Aircraft engine technology course 2022-23. [https://bb.imperial.ac.uk/webapps/blackboard/execute/content/file?cmd=view&content\\_id=\\_2574426\\_1&course\\_id=\\_34885\\_1](https://bb.imperial.ac.uk/webapps/blackboard/execute/content/file?cmd=view&content_id=_2574426_1&course_id=_34885_1), . [Accessed on 27th Jan 2023].
- [4] N. Cumpsty and A. Heyes. *Jet propulsion*. Cambridge University Press, 2015.
- [5] E. Obert. *Aerodynamic Design of Transport Aircraft*. IOS press, 2009.
- [6] aerospaceweb.org. Airliner takeoff speeds. <https://aerospaceweb.org/question/performance/q0088.shtml>. [Accessed on 27th Jan 2023].
- [7] R. Martinez-Botas. Aircraft engine technology coursework task 1. [https://bb.imperial.ac.uk/webapps/blackboard/execute/content/file?cmd=view&content\\_id=\\_2574487\\_1&course\\_id=\\_34885\\_1](https://bb.imperial.ac.uk/webapps/blackboard/execute/content/file?cmd=view&content_id=_2574487_1&course_id=_34885_1), . [Accessed on 15th Jan 2023].
- [8] Airbus. A300 aircraft characteristics for airport planning ac. URL <https://www.airbus.com/sites/g/files/jlcbta136/files/2021-11/Airbus-Commercial-Aircraft-AC-A300-Dec-2009.pdf>. [Accessed on 2nd Feb 2023].
- [9] Rolls-Royce. Ultrafan the ultimate turbofan factsheet. <https://www.rolls-royce.com/~/media/Files/R/Rolls-Royce/documents/innovation/ultrafan-fact-sheet.pdf>. [Accessed on 27th Jan 2023].
- [10] A. El-Sayed, M. Emeara, and M. El Habet. Performance analysis of high bypass ratio turbofan aeroengine, 07 2016.
- [11] J. Kurzke. Gasturb 10 user manual, 2004.
- [12] S. Stapelfeldt. Aircraft engine technology course 2022-23. [https://bb.imperial.ac.uk/bbcswebdav/pid-2719065-dt-content-rid-14089821\\_1/xid-14089821\\_1](https://bb.imperial.ac.uk/bbcswebdav/pid-2719065-dt-content-rid-14089821_1/xid-14089821_1). [Accessed on 27th Jan 2023].
- [13] R. Martinez-Botas. Aircraft engine technology coursework task 2. [https://bb.imperial.ac.uk/bbcswebdav/pid-2574488-dt-content-rid-13422086\\_1/xid-13422086\\_1](https://bb.imperial.ac.uk/bbcswebdav/pid-2574488-dt-content-rid-13422086_1/xid-13422086_1), . [Accessed on 27th Jan 2023].
- [14] D. Evanson, A. Haider, C. Leo, and R. Nag. *Engine Selection and Cycle Analysis of a Fire-Tanker Aircraft*. 2023.
- [15] R. Martinez-Botas. Axial turbine and compressor design supplementary notes. [https://bb.imperial.ac.uk/bbcswebdav/pid-2574477-dt-content-rid-13040456\\_1/xid-13040456\\_1](https://bb.imperial.ac.uk/bbcswebdav/pid-2574477-dt-content-rid-13040456_1/xid-13040456_1), . [Accessed on 17th Mar 2023].
- [16] Romuald Rzadkowski, V.I. Gnesin, and L. Kolodyazhnaya. The influence of the stator-rotor blade number ratio on the aeroelastic behaviour of rotor blades, 04 2012.
- [17] Special Metals Corporation. Inconel alloy 718. [https://bb.imperial.ac.uk/webapps/blackboard/execute/content/file?cmd=view&content\\_id=\\_2574536\\_1&course\\_id=\\_34885\\_1](https://bb.imperial.ac.uk/webapps/blackboard/execute/content/file?cmd=view&content_id=_2574536_1&course_id=_34885_1). [Accessed on 18th Mar 2023].

- [18] C. Davies. Stress analysis of compressor and turbine blades and discs. [https://bb.imperial.ac.uk/webapps/blackboard/execute/content/file?cmd=view&content\\_id=\\_2574538\\_1&course\\_id=\\_34885\\_1](https://bb.imperial.ac.uk/webapps/blackboard/execute/content/file?cmd=view&content_id=_2574538_1&course_id=_34885_1), . [Accessed on 18th Mar 2023].
- [19] R. Martinez-Botas. Aircraft engine technology coursework task 3. [https://bb.imperial.ac.uk/webapps/blackboard/execute/content/file?cmd=view&content\\_id=\\_2574489\\_1&course\\_id=\\_34885\\_1](https://bb.imperial.ac.uk/webapps/blackboard/execute/content/file?cmd=view&content_id=_2574489_1&course_id=_34885_1), . [Accessed on 17th Mar 2023].
- [20] D. Locq and P. Caron. On some advanced nickel-based superalloys for disk applications. *Aerospace Lab*, (3):2, 2011.
- [21] C. Davies. Inconel 718 yield stress-temperature relationship. [https://bb.imperial.ac.uk/webapps/blackboard/execute/content/file?cmd=view&content\\_id=\\_2574535\\_1&course\\_id=\\_34885\\_1](https://bb.imperial.ac.uk/webapps/blackboard/execute/content/file?cmd=view&content_id=_2574535_1&course_id=_34885_1), . [Accessed on 17th Mar 2023].

## A Appendix

### A.1 Labelled Engine Regions

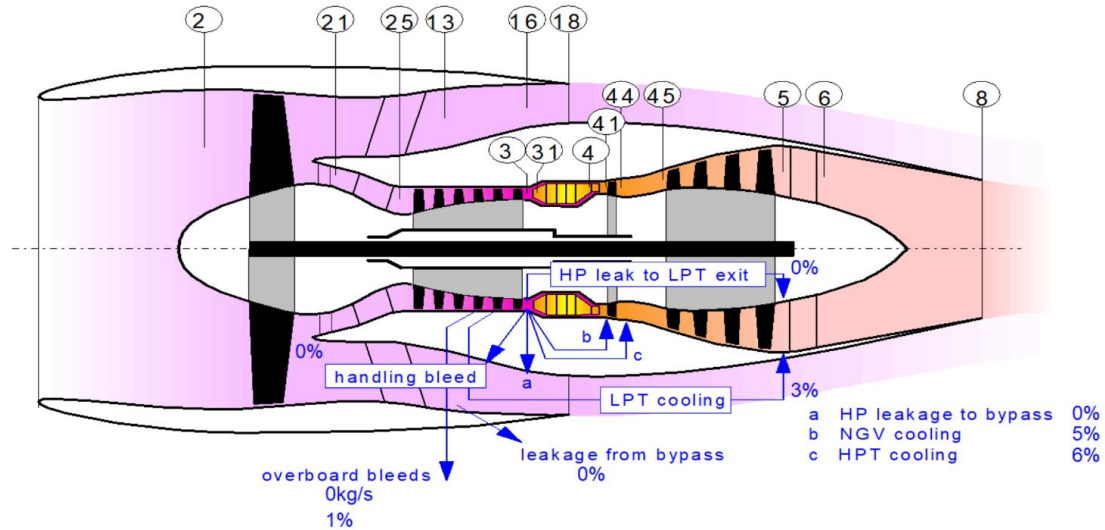


**Figure 17:** Diagram of an engine with labeled regions [3]

### A.2 GasTurb Raw Values

```
Turbofan Alt=10668m / Mn=0.840 ISA
Cruise

Station W T P WRstd FN = 53.20
amb 218.81 23.842 TSFC = 17.0877
2 291.951 249.75 36.721 750.000 WF = 0.90912
13 255.457 300.02 66.097 399.589 BPR = 7.0000
21 36.494 331.86 91.802 43.227 s NOx = 0.5987
25 36.494 331.86 91.802 43.227 Core Eff = 0.5757
3 35.399 758.17 1468.830 3.961 Prop Eff = 0.7331
31 31.020 758.17 1468.830
4 31.929 1725.00 1424.765 5.556 P3/P2 = 40.0000
41 33.754 1677.70 1424.765 5.792 P16/P13 = 0.98000
43 33.754 1299.19 410.468 P16/P6 = 0.79955
44 35.943 1268.72 410.468 P16/P2 = 1.76400
45 35.943 1268.72 402.258 18.998 P6/P5 = 0.98000
49 35.943 901.50 82.668 A8 = 0.35061
5 37.038 892.91 82.668 79.913 A18 = 1.73149
8 37.038 892.91 81.015 81.544 P8/Pamb = 3.39796
18 255.457 300.02 64.775 407.744 P18/Pamb = 2.71683
CD8 = 0.98000
P2/P1= 0.9700
Efficiencies: isentr polytr RNI P/P CD18 = 0.97600
Outer LPC 0.9100 0.9171 0.461 1.800 XM8 = 1.00000
Inner LPC 0.9100 0.9208 0.461 2.500 XM18 = 1.00000
HP Compressor 0.9000 0.9296 0.714 16.000 V18/V8,id= 0.52668 <- !
Burner 1.0000 0.970 Loading % = 100.00
HP Turbine 0.9200 0.9087 0.744 3.471 e444 th = 0.89584
LP Turbine 0.9200 0.9043 0.333 4.866
HP Spool mech 0.9900 Nominal Spd 44000 PWX = 50
LP Spool mech 1.0000 Nominal Spd 13500 WHcl/W25 = 0.06000
Bleed Air: PBld = 1468.83 WLcl/W25 = 0.03000
TBld = 758.2 ZWBld = 0.00000
hum [%] war0 FHV Fuel
0.0 0.00000 43.124 Generic

Input Data File:
C:\Program Files (x86)\ImperialApps\GasTurb\GasTurb10\AET.CYF (modified)
```

**Figure 18:** Cruise Parameters from GasTurb10

Turbofan SL Mn=0.264 ISA

Takeoff (2 Engine)

Station	W	T	P	WRstd	FN	=	180.86
amb		288.15	101.325		TSFC	=	12.1035
2	766.433	292.17	103.165	758.000	WF	=	2.18904
13	670.629	350.71	185.697	403.703	BPR	=	7.0000
21	95.804	387.94	257.912	43.672	s NOx	=	1.6506
25	95.804	387.94	257.912	43.672	Core Eff	=	0.5005
3	92.930	874.98	4126.597	3.976	Prop Eff	=	0.4328
31	81.433	874.98	4126.597				
4	83.623	1750.00	4002.799	5.217	P3/P2	=	40.0000
41	88.413	1706.65	4002.799	5.447	P16/P13	=	0.98000
43	88.413	1264.44	933.820		P16/P6	=	1.47899
44	94.161	1242.21	933.820		P16/P2	=	1.76400
45	94.161	1242.21	915.143	21.646	P6/P5	=	0.98000
49	94.161	805.52	125.557		A8	=	0.74824
5	97.035	802.19	125.557	130.656	A18	=	1.75752
8	97.035	802.19	123.046	133.323	P8/Pamb	=	1.21437
18	670.629	350.71	181.983	411.942	P18/Pamb	=	1.79603
					CD8	=	0.94914
					CD18	=	0.97350
					XM8	=	0.54461
					XM18	=	0.95435
					V18/V8,id	=	1.11555 <- !
					Loading %	=	100.00
					e444 th	=	0.89196
					PWX	=	50
					WHcl/W25	=	0.06000
					WLcl/W25	=	0.03000
					ZWBld	=	0.00000
Bleed Air:	PBld = 4126.60	TBld = 875.0					
hum [%]	war0	FHV	Fuel				
0.0	0.00000	43.124	Generic				

Input Data File:  
C:\Program Files (x86)\ImperialApps\GasTurb\GasTurb10\AET.CYF (modified)

**Figure 19:** Take Off Parameters from GasTurb10

Turbofan SL Mn=0.264 ISA

Takeoff (1 Engine)

Station	W	T	P	WRstd	FN	=	236.95
amb		288.15	101.325		TSFC	=	12.6886
2	876.645	292.17	103.165	867.000	WF	=	3.00656
13	767.065	350.71	185.697	461.755	BPR	=	7.0000
21	109.581	387.94	257.912	49.952	s NOx	=	1.6506
25	109.581	387.94	257.912	49.952	Core Eff	=	0.5111
3	106.293	874.98	4126.597	4.548	Prop Eff	=	0.4000
31	93.144	874.98	4126.597				
4	96.150	1900.00	4002.799	6.250	P3/P2	=	40.0000
41	101.629	1849.97	4002.799	6.518	P16/P13	=	0.98000
43	101.629	1419.86	1078.538		P16/P6	=	0.96456
44	108.204	1389.44	1078.538		P16/P2	=	1.76400
45	108.204	1389.44	1056.967	22.777	P6/P5	=	0.98000
49	108.204	968.38	192.521		A8	=	0.47151
5	111.491	960.61	192.521	107.137	A18	=	2.01025
8	111.491	960.61	188.670	109.324	P8/Pamb	=	1.86203
18	767.065	350.71	181.983	471.179	P18/Pamb	=	1.79603
					CD8	=	0.97905
					CD18	=	0.97350
					XM8	=	1.00000
					XM18	=	0.95435
					V18/V8,id	=	0.58450 <- !
					Loading %	=	100.00
					e444 th	=	0.89473
Bleed Air:	PBld = 4126.60	TBld = 875.0			PWX	=	50
hum [%]	war0	FHV	Fuel		WHcl/W25	=	0.06000
0.0	0.00000	43.124	Generic		WLcl/W25	=	0.03000

Input Data File:  
C:\Program Files (x86)\ImperialApps\GasTurb\GasTurb10\AET.CYF

**Figure 20:** Take Off (Engine Failure) Parameters from GasTurb10

Turbofan Alt=10668m / Mn=0.840 ISA

Top of Climb

Station	W	T	P	WRstd	FN	=	86.16
amb		218.81	23.842		TSFC	=	17.9939
2	443.765	249.75	36.721	1140.000	WF	=	1.55044
13	388.294	300.02	66.097	607.375	BPR	=	7.0000
21	55.471	331.86	91.802	65.705	s NOx	=	0.5987
25	55.471	331.86	91.802	65.705	Core Eff	=	0.5793
3	53.807	758.17	1468.830	6.021	Prop Eff	=	0.7207
31	47.150	758.17	1468.830				
4	48.700	1825.00	1424.765	8.716	P3/P2	=	40.0000
41	51.474	1773.41	1424.765	9.081	P16/P13	=	0.98000
43	51.474	1402.19	446.940		P16/P6	=	0.63473
44	54.802	1366.43	446.940		P16/P2	=	1.76400
45	54.802	1366.43	438.001	27.607	P6/P5	=	0.98000
49	54.802	1007.77	104.134		A8	=	0.44950
5	56.466	996.55	104.134	102.176	A18	=	2.63186
8	56.466	996.55	102.051	104.262	P8/Pamb	=	4.28027
18	388.294	300.02	64.775	619.771	P18/Pamb	=	2.71683
					CD8	=	0.98000
P2/P1=	0.9700				CD18	=	0.97600
Efficiencies:	isentr polytr RNI		P/P		XM8	=	1.00000
Outer LPC	0.9100	0.9171	0.461	1.800	XM18	=	1.00000
Inner LPC	0.9100	0.9208	0.461	2.500	V18/V8,id=	=	0.46272 <- !
HP Compressor	0.9000	0.9296	0.714	16.000	Loading %	=	100.00
Burner	1.0000			0.970	e444 th	=	0.89754
HP Turbine	0.9200	0.9097	0.678	3.188			
LP Turbine	0.9200	0.9063	0.321	4.206			
HP Spool mech	0.9900	Nominal Spd	44000		PWX	=	50
LP Spool mech	1.0000	Nominal Spd	13500		WHcl/W25	=	0.06000
					WLcl/W25	=	0.03000
Bleed Air:	PBld = 1468.83	TBld =	758.2		ZWBld	=	0.00000
hum [%]	war0	FHV	Fuel				
0.0	0.00000	43.124	Generic				

Input Data File:  
C:\Program Files (x86)\ImperialApps\GasTurb\GasTurb10\AET.CYF (modified)

**Figure 21:** Top of Climb Parameters from GasTurb10

### A.3 Blade Cross-sectional Overlays

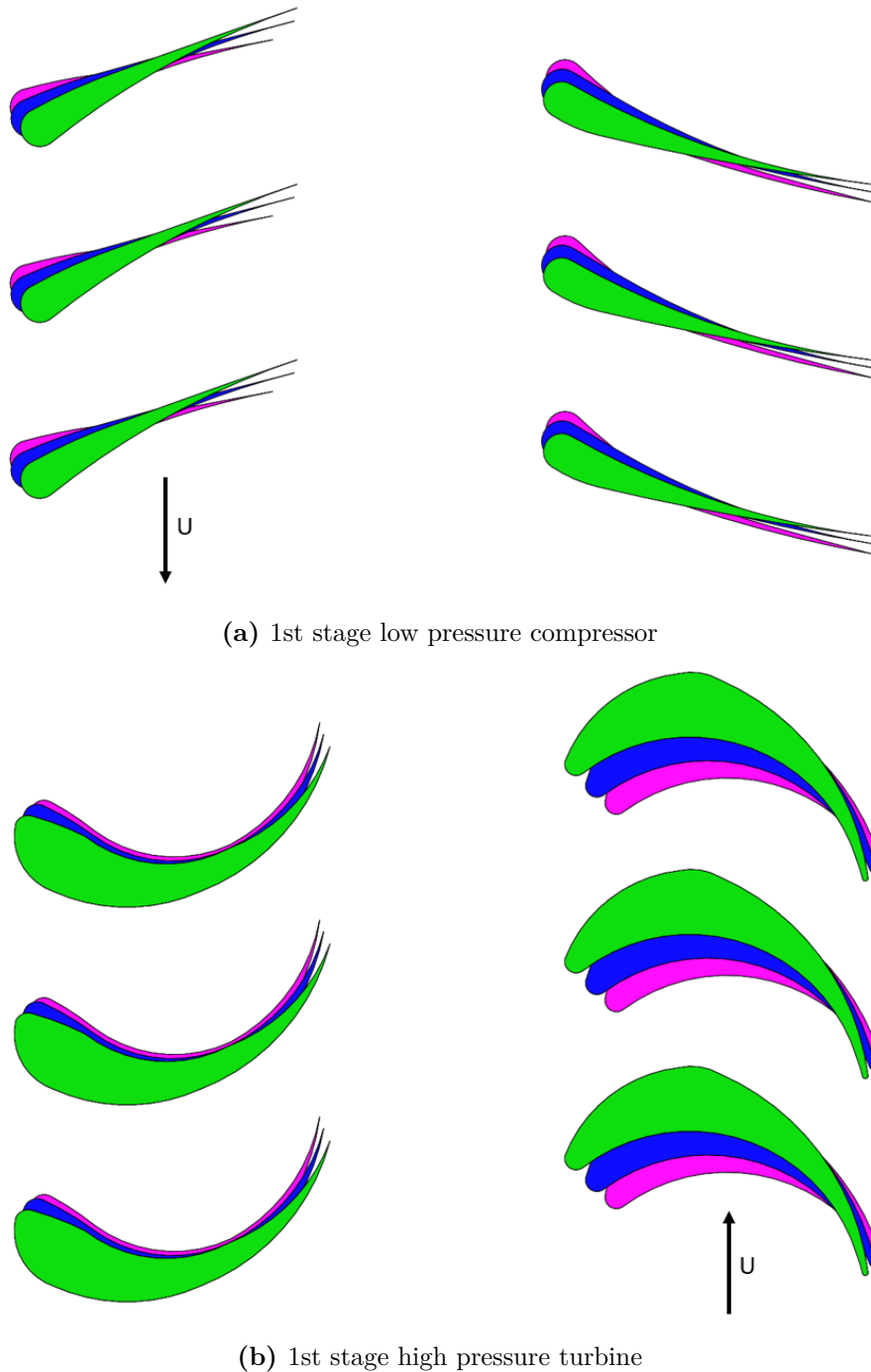


**Figure 22:** Overlays of the cross-sections of blades corresponding to the 1st stage of the LPC (22a) and HPT (22b) at 3 different radii. The radii correspond to hub radius (magenta), mean radius (blue) and tip radius (green).

### A.4 Rim Force Derivation

An infinitesimally small change in centripetal force is described by Equation 59, where an infinitesimally small change in mass,  $dm$  is given by Equation 60. Integrating between the limits of the blade length from root to tip yields the integral in Equation 61 which in turn results in the expression in 62.

$$dF = \Omega^2 r dm \quad (59)$$

$$dm = \rho c t dr \quad (60)$$

$$\int_{-F_{rim}}^0 dF = \Omega^2 \rho c t \int_{R_i}^{R_o} dr \quad (61)$$

$$F_{rim} = \Omega^2 \rho c t L_{blade} \left( r_i + \frac{L_{blade}}{2} \right) \quad (62)$$

## A.5 GitHub Code Repository

The code used for the design and optimization of the engine can be found at this [repository](#).

## A.6 Code Architecture

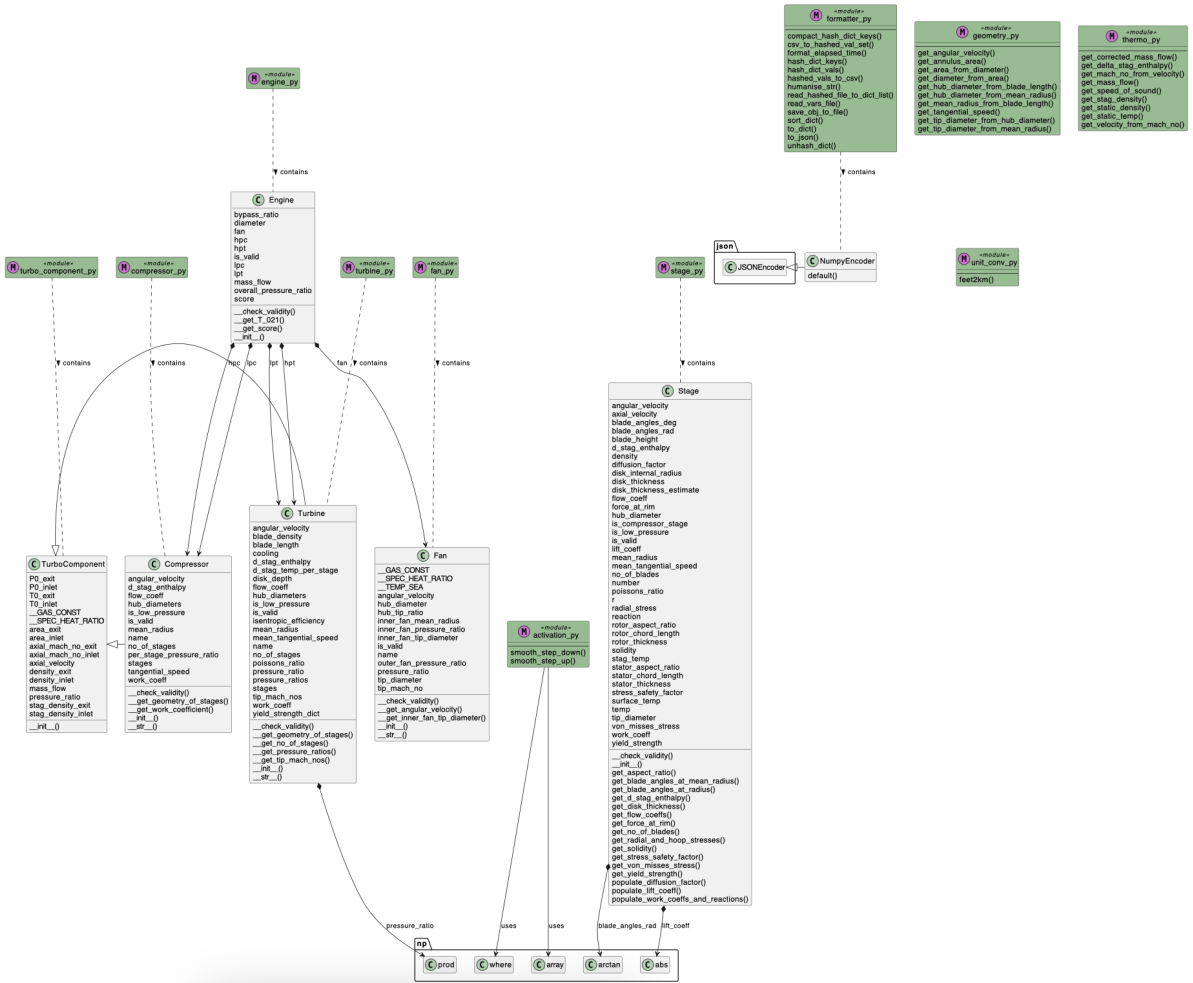


**Figure 23:** UML diagram of code showing nested class system used.

## A.7 Final Engine All Parameters

All properties of the final engine design can be found at this [JSON file](#).